HOKKAIDO UNIVERSITY

| | |
|---|---|
| Title | Essential roles of cholesterol-binding membrane protein TSPO2 in maturation and proliferation of erythroblasts in mice |
| Author(s) | Benjaporn, KIATPAKDEE |
| Degree Grantor | 北海道大学 |
| Degree Name | 博士(獣医学) |
| Dissertation Number | 甲第14273号 |
| Issue Date | 2020-09-25 |
| DOI | https://doi.org/10.14943/doctoral.k14273 |
| Doc URL | https://hdl.handle.net/2115/79703 |
| Type | doctoral thesis |
| File Information | Benjaporn.pdf |




Hokkaido University Collection of Scholarly and Academic Papers : HUSCAP

# Essential roles of cholesterol-binding membrane protein TSPO2 in maturation and proliferation of erythroblasts in mice

(マウス赤芽球の成熟と増殖におけるコレステロール結合蛋白質 TSPO2 の役割)

**Benjaporn Kiatpakdee**

*Laboratory of Molecular Medicine, Department of Veterinary Clinical Sciences*

*Graduate School of Veterinary Medicine, Hokkaido University*

# Contents

**Abbreviations**

**Preface**..... 1

**Introduction**..... 3

**Materials and Methods**..... 6

**Results**..... 15

**1. Erythroid cell maturation in *Tspo2* knockout mice**..... 15

**2. Erythroid cell maturation and proliferation in *Tspo2* knockout cell line**... 22

**Discussion**..... 36

**References**..... 42

**Acknowledgements**..... 48

**Abstract**..... 49

**Abstract in Japanese**..... 51

# Abbreviations

Abbreviations used in this study are as follows:

| | |
|---|---|
| RBC | red blood cell |
| TSPO2 | translocator protein 2 |
| TSPO | translocator protein |
| HK | high potassium ion |
| LK | low potassium ion |
| Na,K-ATPase | $Na^+$- and $K^+$-dependent adenosine triphosphatase |
| MEDEP | mouse ES cell-derived erythroid progenitor |
| BM | bone marrow |
| CEs | cholesteryl esters |
| ER | endoplasmic reticulum |
| MCV | mean corpuscular volume |
| MCH | mean corpuscular hemoglobin |
| MCHC | mean corpuscular hemoglobin concentration |
| Hb | hemoglobin |
| Hct | hematocrit |
| PCR | polymerase chain reaction |
| SDS-PAGE | sodium dodecyl sulfate-polyacrylamide gel electrophoresis |
| CFU-E | colony forming unit-erythroid |
| PBS | phosphate buffered saline |
| FACS | fluorescence-activated cell sorting |

| | |
|---|---|
| FITC | fluorescein isothiocyanate |
| APC | allophycocyanin |
| PE | phycoerythrin |
| PEcy7 | phycoerythrin-cyanine 7 |
| NBD-cholesterol | 22-(N-(7-Nitrobenz-2-oxa-1,3-diazol-4-yl)amino)-23,24-bisnor-5-cholen-3β-ol |
| MFI | median fluorescence intensity |
| *Hba* | murine $\alpha$-globin gene |
| *Hbb* | murine $\beta$-globin gene |
| *TfR* | murine transferrin receptor gene |
| *Alas1* | murine 5'-aminolevulinate synthase 1 gene |
| *Alas2* | murine 5'-aminolevulinate synthase 2 gene |
| *Gata1* | murine globin transcription factor 1 gene |
| *Gata2* | murine globin transcription factor 2 gene |
| *Klf1* | murine Krüppel-like factor 1 gene |
| *Setd8* | murine histone methyltransferase gene |
| *Slc4a1* | murine anion exchanger 1 (band 3) gene |
| *Gapdh* | murine glyceraldehyde-3-phosphate dehydrogenase gene |

# Preface

Erythropoiesis is an essential process that produces sufficient numbers of the enucleate red blood cell (RBC) from the erythroid precursor cell. This process proceeds through inexorably linked terminal maturation and cell proliferation of erythroblasts. The mechanisms for various changes during erythropoiesis including nuclear condensation, enucleation, expulsion of organelles, and the plasma membrane remodeling are directly relevant to pathobiology of various anemias, precise evaluation of different hematologic conditions, and improving *ex vivo* production of functional RBCs for therapeutics. However, the factors implicated in regulation of maturation and proliferation in erythroblasts remain yet to be fully defined.

In general, carnivore animals possess mature RBCs (erythrocytes) with low intracellular $K^+$ concentration (LK RBCs) because of total loss of Na,K-ATPase during reticulocyte maturation into erythrocytes. However, some dogs have RBCs with high $K^+$ concentration (HK RBCs) because they retain Na,K-ATPase in their morphologically matured erythrocytes. The HK RBC phenotype in dogs, an autosomal recessive trait, is accompanied with various characteristics of erythroid precursor cells, including the persistence of immature-type glycolytic isozymes and increased energy consumption. Hence, HK RBC phenotype likely represents an impaired regulation in orderly maturation of erythroblasts and the molecular basis of the HK trait would provide clues to some aspects of erythropoiesis.

We previously identified the mutations in the cholesterol-binding membrane protein translocator protein 2 (TSPO2) gene as the molecular cause for HK RBC trait, and found that maturation and cytokinesis of erythroblasts from HK dogs were impaired. The purpose of the present study was to examine if the TSPO2 function was indeed involved in normal

erythropoiesis. To pursue this, the effects of the *Tspo2* knockout on erythropoiesis were investigated in mice and in a murine erythroid precursor cell line. The findings of the present study demonstrate that TSPO2 function is essential in coordination of erythroblast maturation, cell-cycle progression, cytokinesis, and cell proliferation to ensure efficient erythropoiesis.

The present study has been accepted for publication as described below.

1) Kiatpakdee, B., Sato, K., Otsuka, Y., Arashiki, N., Chen, Y., Tsumita, T., Otsu, W., Yamamoto, A., Kawata, R., Yamazaki, J., Sugimoto, Y., Takada, K., Mohandas, N., and Inaba, M. (2020) Cholesterol-binding protein TSPO2 coordinates maturation and proliferation of terminally differentiating erythroblasts. *Journal of Biological Chemistry* (in press, doi: 10.1074/jbc.RA119.011679)

# Introduction

Erythropoiesis is a critical process that produces sufficient numbers of the enucleate red blood cell (RBC) from the erythroid precursor cell. This process proceeds through inexorably linked terminal maturation and cell proliferation of erythroblasts, and is tightly regulated by the cooperation among mitogenic, differentiating, and antiapoptotic factors (Dzierzak and Philipsen 2013; Papayannopoulou and Migliaccio, 2017). Recent advances as well as earlier studies have defined the mechanisms for various changes during erythropoiesis including nuclear condensation (Malik et al., 2017), enucleation (Konstantinidis et al., 2012; Gnanapragasam et al., 2016; Swartz et al., 2016; Zhao et al., 2016), organelles expulsion (Holm et al., 2014; Moras et al., 2017), and the plasma membrane remodeling (Lazarides and Moon, 1984; Hanspal and Palek, 1987; Mohandas and Gallagher, 2008). These findings are directly relevant to pathobiology of various anemias, precise evaluation of different hematologic conditions, and improving *ex vivo* production of functional RBCs for therapeutics. However, the factors implicated in regulation of maturation and proliferation in erythroblasts remain yet to be fully defined, although previous studies have documented several genetic factors that determine the RBC traits in humans (Sankaran et al., 2012).

Cation contents in mature RBCs (erythrocytes) are quite different among species (Chan et al., 1964). Human and rodent erythrocytes possess high Na,K-ATPase activity resulting in high intracellular $K^+$ concentration (HK RBCs). In contrast, canine erythrocytes have low $K^+$ concentration (LK RBCs) because they totally lose red cell Na,K-ATPase during reticulocyte maturation into erythrocytes (Maede and Inaba, 1985; Inaba and Maede, 1986; Komatsu et al., 2010). However, some dogs possess HK RBCs because they retain Na,K-ATPase in their erythrocytes (Maede et al., 1983; Maede and Inaba, 1985; Inaba and Maede, 1986). This HK phenotype is inherited in an autosomal recessive manner and is accompanied with various

characteristics of erythroid precursor cells, including the persistence of immature-type glycolytic isozymes and increased energy consumption (Maede and Inaba, 1987; Inaba and Maede, 1989). Hence, HK RBC phenotype likely represents an impaired regulation in orderly maturation of erythroblasts and the molecular basis of the HK trait would provide clues to some aspects of erythropoiesis.

Previously, we performed genome-wide linkage analysis to clarify the mechanism for the HK RBC trait, and identified two independent mutations, namely C40Y and VFT mutations, in the translocator protein 2 (TSPO2) gene as the molecule cause for the HK trait (Kiatpakdee et al., in press). TSPO2 has been recognized as a paralogue of TSPO (Fan et al., 2009). TSPO is an 18-kDa five membrane-spanning protein which is previously known as PBR (peripheral-type benzodiazepine receptor) with cholesterol- and drug-binding domain and localized primarily in the outer mitochondrial membrane in various tissues. TSPO has been implicated in various functions in mammalian cells including cholesterol and heme transport, steroid hormone synthesis, mitochondrial respiration, permeability transition pore opening, cell apoptosis, and cell proliferation (Gavish et al., 1999; Papadopoulos et al., 2006; Azarashvili et al., 2007; Li et al., 2007; Fan et al. 2012). In contrast to TSPO, TSPO2 shows erythroid-specific expression and localization at the endoplasmic reticulum (ER), nuclear, and plasma membranes (Fan et al., 2009; Marginedas-Freixa et al., 2016). It has the ability to bind cholesterol and is involved in cholesterol redistribution or transport during erythropoiesis (Fan et al., 2009). Intriguingly, impaired reticulocyte maturation due to markedly increased cellular cholesterol (Holm et al., 2014) and a role for lipid raft assembly with GTPases and F-actin in enucleation (Konstantinidis et al., 2012) indicate the importance of cholesterol homeostasis. Furthermore, hypocholesterolemia in patients of chronic anemias suggests increased cholesterol requirements for erythroid cell expansion (Shalev et al., 2007). However, the roles of cholesterol metabolism in regulating erythropoiesis has not been fully defined.

Based on unexpected finding that the HK trait is associated with the *TSPO2* mutations, we examined erythropoiesis in HK dogs and found morphological abnormalities in maturing erythroblasts (Kiatpakdee et al., in press). In brief, the cells from bone marrow (BM) aspirates showed the presence of abundant numbers of binucleated erythroblasts at different developmental states, basophilic, polychromatic, and orthochromatic erythroblasts in HK dogs, indicative of a cell-division defect. When BM cells were cultured in the presence of erythropoietin (EPO), HK orthochromatic erythroblasts shed nuclei with morphologically incomplete chromatin condensation, and the sizes of expelled pyrenocytes and nascent reticulocytes were larger than those of LK cells. Moreover, HK cells showed various abnormal morphological features, involving binucleated cells, long intercellular bridges, abnormal cell division, and apoptotic appearance. These data suggested that the TSPO2 mutations impaired maturation and cytokinesis during late stages of terminal erythroid differentiation.

To further clarify the roles of TSPO2 in erythropoiesis, in the present study, the effects of the TSPO2 defect on erythropoiesis were investigated in mice and in a murine erythroid precursor cell line MEDEP-BRC5 (Hiroyama et al., 2008) which exhibited terminal differentiation most similar to primary mouse erythroid cells among several murine erythroid cell line (Gautier et al., 2020). We first analyzed hematological phenotypes in *Tspo2* knockout mice (*Tspo2*$^{-/-}$) and found that the TSPO2 defects had dominant effects in erythropoiesis, exhibiting modest and compensated anemia in *Tspo2*$^{-/-}$ mice with impaired cytokinesis, increased binucleated erythroblasts, and increased Na,K-ATPase contents in their RBC membranes. Then, *Tspo2*-deficient MEDEP cells showed similar cytokinesis failure, decreased cell proliferation, delayed cell-cycle progression and maturation, and a depletion in cellular cholesterol. These findings demonstrate that TSPO2 function is essential in coordination of erythroblast maturation, cell-cycle progression, cytokinesis, and cell proliferation to ensure efficient erythropoiesis.

# Materials and Methods

## Production of *Tspo2* knockout mice

The *Tspo2* mutant mice were generated by CRISPR/Cas9-mediated gene knockout (Yang et al., 2014) by injecting the exon 3-specific sgRNA (5'-CTTTGTAGGTGTGCCC-3'), Cas9 mRNA, and the single strand donor DNA (5'-CTTTGTAGGTGTGCCCtaatagactagtctagCTGcag-3') into the pronucleus of embryos of C57BL/6 mice. The donor DNA contained several mutations to create terminating codons and restriction sites (lowercase) at the targeted region. The founder mouse obtained was compound heterozygous for a deletion mutation of 105 nucleotides (Δ105, g.1374_1478del) and an insertion mutation of 2 nucleotides (Ins2, g.1486_1487insCG). This mouse was backcrossed to C57BL/6 mice to generate heterozygous (*Tspo2*$^{+/-}$) offspring for two independent mutations Δ105 and Ins2, and mice were crossed within the same strain to obtain wild-type (*Tspo2*$^{+/+}$), heterozygous (*Tspo2*$^{+/-}$), and homozygous (*Tspo2*$^{-/-}$) progeny. In the present study, we used mice with the Δ105 mutation. Mouse were genotyped by PCR using primers mTspo2ex1F (5'-ATGCAGCTTCAAGGACCTGTCTT-3') and mTspo2ex1R (5'-CCATGACAGAGTAGATGGTCACC-3') followed by digestion of the PCR products with *Pst* I (Fig. 1).

Mice were kept at the animal experimentation facility of Graduate School of Veterinary Medicine, Hokkaido University. All experimental procedures were reviewed and approved by the Laboratory Animal Experimentation Committee, Graduate School of Veterinary Medicine, Hokkaido University with approval number 15-0019.

## Sample collection

Mice were euthanized with $CO_2$ and measured for their body weights. Blood was collected by cardiac puncture using a 27G needle and anticoagulated with EDTA/$K_2$. Spleens and femurs were collected as well and kept on ice.

## Complete blood count and reticulocyte count

The complete blood count was performed for blood from mice using hematology analyzer ProCyte (IDEXX Laboratories). Reticulocytes were stained with new methylene blue (Terumo) and counted for reticulocytes under microscopy at the magnification of × 1,000.

## Morphology of bone marrow cells

Bone marrow (BM) cells were isolated from femur by flushing with phosphate-buffered saline (PBS) through a 23G needle and cytospin smears of cells were stained with Wright-Giemsa (Wako) for morphological examination. The size of extruded nuclei (pyrenocytes) and nascent reticulocytes generated by enucleating cells were determined using ImageJ (NIH).

## Flow cytometry of bone marrow cells

Immunophenotype staining and FACS analysis of BM cells were performed as reported previously (Chen et al., 2009; Liu et al., 2015). Briefly, BM cells were washed in PBS containing 0.2% (w/v) bovine serum albumin (PBS/0.2% BSA) and stained with PE-conjugated anti-CD71 (BD Pharmingen), FITC-conjugated anti-TER119, PE-Cy7-conjugated anti-CD44, and APC-conjugated anti-CD45.2/Gr1/CD11b antibodies (all from BioLegend). Cells were washed twice after incubation in the dark at 4℃ for 30 minutes and stained with the cell

viability marker propidium iodide (PI) and analyzed by FACSVerse flow cytometer (BD Bioscience). Data were analyzed by FlowJo V10 (FlowJo).

## Preparation of *Tspo2*$^{-/-}$ MEDEP-BRC5 cell line

MEDEP-BRC5 cells (MEDEP cells, Hiroyama et al., 2008) were purchased from Riken Bioresource Research Center (Tsukuba, Japan). *Tspo2*$^{-/-}$ MEDEP cells were generated by CRISPR/Cas9-mediated gene knockout technique (Cong et al., 2013). Briefly, mouse *Tspo2* exon 1-specific sgRNA (5'-GTCAGCATCCAGTCGGGTGTG-3') was inserted into *Bbs* I-treated pX330-U6-Chimeric_BB-Cbh-hSpCas9 (Addgene). MEDEP cells were transfected with this plasmid and pCDH-CMV-MCS-puro (Addgene). Two days later, cells were selected for 48 hours with 1 μg/ml puromycin and cloned by limiting dilution. We obtained two independent clones of *Tspo2*$^{-/-}$ cells. The clone KO13 was compound heterozygous for p.Arg29fs (c.85_88del) that resulted in a premature termination and p.Ser27X (c.80_90del) mutations. The other clone KO26 was homozygous for p.Cys30X (c.89_90del) mutation. Since clones KO13 and KO26 showed impairments similar to each other in cell proliferation and hemoglobinization, further studies were carried out on the clone KO13.

## Culture and induction into terminal erythroid differentiation of MEDEP cells

The control and *Tspo2*$^{-/-}$ MEDEP cells were maintained and induced into terminal differentiation as reported previously (Hiroyama et al., 2008). Briefly, the cells were maintained in Iscove's Modified Dulbecco's medium (IMDM, SIGMA) supplemented with 15% fetal bovine serum (Biowest), 10 μg/ml human insulin, 5.5 μg/ml human transferrin, 5 ng/ml sodium selenite (ITS liquid MEDIA supplement, Sigma), 0.45 mM α-monothioglycerol (Sigma), 50

ng/ml mouse stem cell factor (Miltenyl Biotec), 50 μg/ml ascorbic acid (Sigma), 1 μM dexamethasone (Nippon Zenyaku Kogyo), 100 unit/ml penicillin, 100 μg/ml streptomycin, and 2 mM L-glutamine (Wako) at 37℃ and 5% $CO_2$.

When the cells were induced into terminal differentiation, cells were washed twice with warmed PBS and resuspended at the level of $1 \times 10^6$ cells/ml in the induction medium consisting of IMDM supplemented with 15% fetal bovine serum, 10 μg/ml human insulin, 5.5 μg/ml human transferrin, 5 ng/ml sodium selenite, 100 unit/ml penicillin, 100 mg/ml streptomycin, 2 mM L-glutamine, 0.45 mM α-monothioglycerol, 10 U/ml erythropoietin (EPO, Kyowa Kirin), and 50 μg/ml ascorbic acid (Sigma). The cells were incubated at 37℃ and 5% $CO_2$. Pyrenocyte and reticulocyte sizes were measured as described above.

## Analyses of morphology, enucleation rate, and hemoglobinization in MEDEP cells

Cytospin smears of MEDEP cells were stained with Wright-Giemsa for morphological examination. The size of pyrenocytes was measured by ImageJ. Enucleation rate was checked by counting enucleated cells at 48 hours after induction into terminal differentiation.

For measurement of hemoglobin, a total of $1 \times 10^6$ cells was harvested at the appropriate time intervals. The cells were washed with PBS, pelleted, and kept at −80℃. before further analysis. Hemoglobin concentration was measured as described previously (Cioe et al., 1981). Cells were suspended in distilled water, lysed by three cycles of freeze-thawing, and centrifuged at 18,000 × g for 10 minutes. The supernatants were measured for the absorbance at 414 nm using spectrophotometer Beckman DU® 640, assuming an absorbance of 1.0 at 414 nm is equivalent to 0.094 mg/ml of hemoglobin. Hemoglobin concentration (pg/cell) was normalized by cell number counted on a hemocytometer.

## Flow cytometry of MEDEP cells in erythroid maturation

MEDEP cells in culture (0.5 to 1 x $10^6$ cells) were collected at 0, 12, 24, and 48 hours following induction. Cells were washed in PBS/0.2 % BSA twice and incubated with biotin-labeled anti-mouse CD71 antibody (0.5 µg/ml, BD Pharmingen), PE-labeled anti-mouse TER119 antibody (0.5 µg/ml, Tonbo Biosciences), and PE-Cy7-labeled anti-mouse CD44 antibody (0.5 µg/ml, Tonbo Biosciences) for 30 minutes in the dark. After washing once with PBS/0.2 % BSA, APC- labeled streptavidin (Ebioscience) was added to yield the final concentration of 1 µg/ml and incubated on ice for 30 minutes in the dark. Finally, cells were washed twice and resuspended in PBS/0.2 % BSA and stained with PI at the concentration of 1 µg/ml and analyzed on a FACSVerse flow cytometer. Data were analyzed by FlowJo V10 software.

## Analyses of cell division, cell cycle, and apoptotic cell death

Flow cytometric analysis for cell division using CellTrace Violet (Thermo Fisher) was carried out as recommended by the manufacturer and the number of cell divisions was estimated as previously reported (Sankaran et al., 2012). A total of 1 × $10^6$ MEDEP cells were collected and washed twice in PBS. Cells were suspended in IMDM without fetal bovine serum and stained with 2.5 µM CellTrace™ Violet (ThermoFisher) at 37℃ for 10 minutes. The cells were washed and resuspended in the induction medium and incubated at 37℃ and 5% $CO_2$. At appropriate time intervals, cells were harvested and analyzed using a FACSAriaII cell sorter (BD Biosciences). Data were analyzed by FlowJo V10 software.

For cell cycle analysis, cells were harvested and washed in PBS followed by fixation in chilled 70% ethanol in PBS for 2 hours. Cells were washed twice and resuspended in PBS, and

incubated at 37℃ for 30 minutes in the presence of RNase (Omega Bio-Tek) at the concentration of 250 μg/ml. To this was added PI at the concentration of 50 μg/ml and the cells were kept on ice for 30 minutes followed by flow cytometric measurement on a FACSVerse flow cytometer. Data were analyzed by FlowJo software.

Apoptotic cell death was analyzed by flow cytometry using Annexin V-FITC apoptosis detection kit (BioVision). Briefly, $6 \times 10^5$ cells were harvested on day 3 in induction culture, suspended in PBS/0.2 % BSA, and filtered through a nylon mesh (Kyoshin Rikoh Inc.). Annexin V-FITC solution was added to the cell suspension at the ratio of 4 μl/ml and the cells were incubated for 5 minutes on ice. Fluorescence intensities were measured on a FACSVerse flow cytometer and the data were analyzed using FlowJo. The cells that were incubated in the presence of 100 μM cycloheximide (Wako) for 4 hours prior to sampling were used as the control for the apoptotic cells.

## Cholesterol uptake and intracellular distribution in MEDEP cells

The uptake of cholesterol was measured using 25-NBD-cholesterol (Avanti polar lipids) as described previously (Fan et al., 2009). Intracellular unesterified cholesterol and cholesteryl esters (CEs) were stained with filipin III using a Cholesterol cell-based detection assay kit (Cayman Chemical) and Nile Red (Wako Pure Chemical Industries, Ltd.), respectively, following the manufacturers' protocols. After fixation of the cells, these specimens were mounted with ProLong Gold Antifade (Thermo Fisher Scientific) for fluorescent microscopy.

## Immunoblotting

Preparation of RBC membrane ghosts, determination of membrane protein contents, and immunoblotting analysis were performed as described previously (Inaba and Maede, 1988; Ito et al., 2006). Briefly, the RBC membrane ghosts were prepared by hypotonic lysis and washes in 5 mM Tris/Cl (pH 7.8), 1 mM EDTA, and 0.2 mM phenylmethylsulfonyl fluoride at 4℃. Protein concentration of the membranes was determined with a protein assay BCA kit (Nacalai tesque) using bovine serum albumin as the standard. RBC membrane proteins were separated by SDS-polyacrylamide gel electrophoresis (PAGE) with 12% polyacrylamide gels followed by immunoblotting using the anti-canine Na,K-ATPase α-subunit antibody (Inaba and Maede, 1986). Signals were detected using the ECL chemiluminescence detection system with horse radish peroxidase substrate (Millipore) on an Image Quant LAS 4000 mini image analyzer (GE Healthcare) and the signal intensities were quantitated using Image Quant TL software (GE Healthcare).

## Analysis for expressions of erythroid-specific genes in MEDEP cells

A total of $1 \times 10^6$ cultured cells was pelleted, washed with PBS, and kept at −80℃ until analysis. Total RNAs were extracted from the cells using an RNeasy Mini kit (QIAGEN) following the protocol from the manufacturer. cDNA was synthesized using a high capacity cDNA reverse transcription kit (Applied Biosystems). The quantitative PCR analysis was performed with Power SYBR Green PCR master mix (Applied Biosystems) and primers for amplification of each gene shown in Table 1 using the Light Cycler 96 System (Roche Diagnostics).

## Statistical analysis

Statistical evaluation between experimental groups was performed using the data analysis tool in GraphPad Prism (unpaired *t*-test or Mann-Whitney *U* test for nonparametric data). All analyses were considered statistically significant at $P < 0.05$.

**Table 1. Oligonucleotide primers used for quantitative PCR reactions**

Primers for mRNA expression analysis in MEDEP cell line were designed and checked for specificity before examination. Each primer pair consists of forward and reverse sequences.

| Gene | Species | GenBank Accession number | Sequence |
|---|---|---|---|
| *Gapdh* | *Mus musculus* | NM_001289726 | Forward: 5'- GTCTTCACCACCATGGAGAAG -3' |
| | | | Reverse: 5'-GCCATCCACAGTCTTCTGGGT-3' |
| *Tspo2* | *Mus musculus* | NM_027292.2 | Forward: 5'-ACCGACTGGATGGCTGATGAATGA-3' |
| | | | Reverse: 5'-ATTGGGCAGACCAACCTGGATCTT-3' |
| *Hba* | *Mus musculus* | NM_008218.2 | Forward: 5'-CTCTCTGGGGAAGACAAAAGC-3' |
| | | | Reverse: 5'-GGTGGCTAGCCAAGGTCACCA-3' |
| *Hbb* | *Mus musculus* | NM_001278161.1 | Forward: 5'-TTCTGACATAGTTGTGTTGACTCAC-3' |
| | | | Reverse: 5'-TCGGAGTTCACCTTTCCCCA-3' |
| *Alas1* | *Mus musculus* | NM_001291835.1 | Forward: 5'-CGAGTCACATCATCCCTGTG-3' |
| | | | Reverse: 5'-TTAAGTTCCAGCCCAACTCG-3' |
| *Alas2* | *Mus musculus* | NM_009653.3 | Forward: 5'-ATCTGTGCGCCTACTCAAGG-3' |
| | | | Reverse: 5'-TGTGCTTGGAGAGCAGAAGA-3' |
| *Gata1* | *Mus musculus* | NM_008089.2 | Forward: 5'-CAGAACCGGCCTCTCATCC-3' |
| | | | Reverse: 5'-TAGTGCATTGGGTGCCTGC-3' |
| *Gata2* | *Mus musculus* | NM_008090.5 | Forward: 5'-GAATGGACAGAACCGGCC-3' |
| | | | Reverse: 5'-AGGTGGTGGTTGTCGTCT-3' |
| *Slc4a1* | *Mus musculus* | NM_011403.2 | Forward: 5'-TATGGGGTCGCCCACATCTAT-3' |
| | | | Reverse: 5'-AGGCCGAATCTGATCCTCGTA-3' |
| *Klf1* | *Mus musculus* | NM_010635.3 | Forward: 5'-AGAGTGGATCCAAGGACCGT-3' |
| | | | Reverse: 5'-CCTCTGGTCTAGGGGTCCAT-3' |
| *Setd8* | *Mus musculus* | NM_030241.3 | Forward: 5'-CAGACCAAACTGCACGACATC-3' |
| | | | Reverse: 5'-CTTGCTTCGGTCCCCATAGT-3' |

# Results

## 1. Erythroid cell phenotypes in *Tspo2* knockout mice

Based on the finding that HK dog erythroblasts with *TSPO2* mutations exhibited a cell division defect and morphological abnormalities in terminal maturation, we attempted to gain further insight into the role of TSPO2 defect on erythropoiesis. For this purpose, the germline *Tspo2*-knockout mice with the Δ105 mutation were produced (Fig. 1) and hematopoiesis in *Tspo2*-deficient mice was examined.

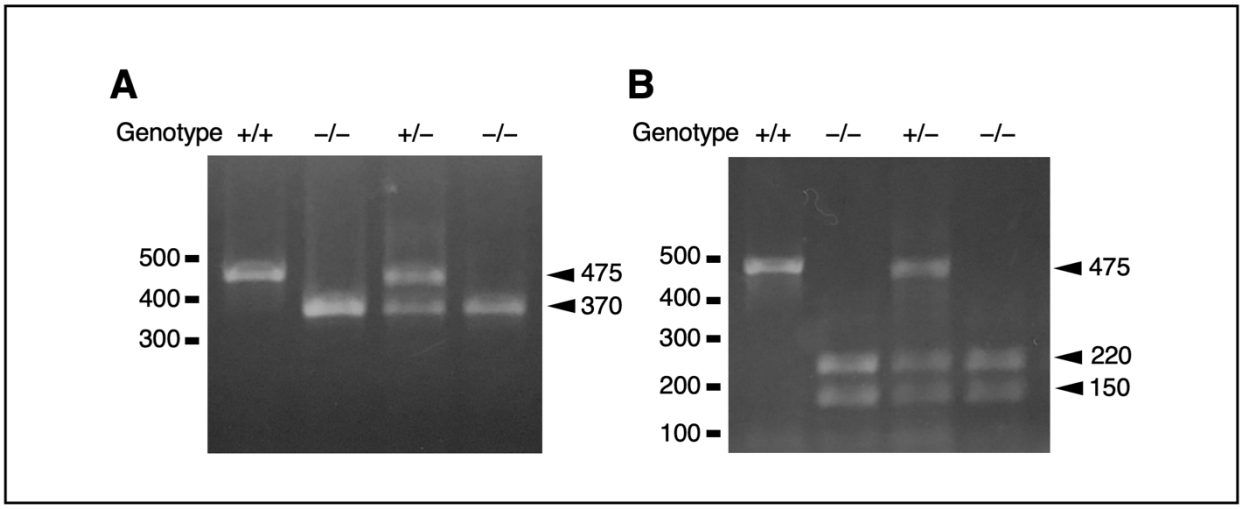
Adult *Tspo2*$^{-/-}$ mice at 20 weeks of age showed significant reduction in RBC count, hemoglobin concentration, and hematocrit values and a marked increase in reticulocyte count compared to age-matched *Tspo2*$^{+/+}$ mice, while no remarkable difference was noted in the mean corpuscular volume and the mean corpuscular hemoglobin (Fig. 2A). The 20-week-old *Tspo2*$^{-/-}$ mice also exhibited an increased spleen size (Fig. 2B), suggesting an enhanced extramedullary erythropoiesis to expand the capacity of RBC production in the spleen (Socolovsky, 2007; Paulson et al., 2011; Liu et al., 2015). In addition, *Tspo2*$^{-/-}$ mice at 6~8 weeks of age showed a significant reduction in hematocrit value and a marked increase in reticulocyte count compared to *Tspo2*$^{+/+}$ mice (Fig. 2C). It should be noted that heterozygous *Tspo2*$^{+/-}$ mice at 20 weeks of age also showed a mild but significantly reduced RBC counts (Fig. 2A). These data demonstrate that *Tspo2*$^{-/-}$ mice have a well-compensated mild anemia and suggest that the anemic phenotypes due to *Tspo2* aberration is dominant.

Na,K-ATPase contents in RBC membranes from *Tspo2*$^{-/-}$ mice were significantly higher than those in control *Tspo2*$^{+/+}$ mice (0.97 ± 0.38 vs. 0.27 ± 0.11 for the relative abundance, mean ± S.D., n = 3, Fig. 3), consistent with the RBC phenotype in HK dogs (Inaba and Maede, 1986; Komatsu et al., 2010).

To clarify the cause of regenerative anemia in *Tspo2*-deficient mice, cellular features of BM-derived erythroid cells from adult mice were examined. In BM cells, both *Tspo2*$^{-/-}$ and *Tspo2*$^{+/-}$ mice had a marked increase in binucleated erythroblasts, indicative of a cell-division defect. The major population (approximately 70%) of binucleated cells contained polychromatic and orthochromatic erythroblasts (Figs. 4A and 4B). The size of expelled nuclei (pyrenocytes) in *Tspo2*$^{-/-}$ mice was significantly larger than that in *Tspo2*$^{+/+}$ mice (Figs. 4C and 4D). Flow cytometric analysis of cell surface marker CD44 together with forward scatter in BM-derived TER119-positive cells from age-matched *Tspo2*$^{+/+}$ and *Tspo2*$^{-/-}$ mice showed similar profiles (Fig. 5A). These cells could be divided into six fractions with different maturation stages as reported previously (Chen et al., 2009; Liu et al., 2015). Consistent with the increase in their binucleated erythroid cells, relative abundance of populations III and IV, corresponding to polychromatic and orthochromatic erythroblasts, respectively, was significantly higher, with concordant decrease of erythrocytes in faction VI, in *Tspo2*$^{-/-}$ mice than in *Tspo2*$^{+/+}$ mice (Fig. 5B).

These hematological and morphological features in *Tspo2*$^{-/-}$ mice are very similar to erythroid phenotypes observed in HK dogs (Kiatpakdee et al., in press) and demonstrate that the *Tspo2* defect predominantly impairs cytokinesis of erythroblasts and causes differentiation defects between the basophilic and orthochromatic stages, leading to ineffective erythropoiesis and mild compensated anemia.

**Figure 1. Genotyping of *Tspo2* knockout mice**




**A.** The *Tspo2* knockout mice with the Δ105 mutation were genotyped by PCR followed by digestion of the PCR products with *Pst* I. PCR amplification of genomic DNA generated 475-bp and 370-bp fragments from the wild-type and Δ105 mutant alleles, respectively, so that we could identify the genotypes for *Tspo2* as the wild-type (+/+) and heterozygous (+/−) and homozygous (−/−) for the Δ105 mutation. **B.** The Δ105 mutation was confirmed by digestion with *Pst* I, since the Δ105 mutation created a *Pst* I restriction site in the mutated allele. The 475-bp fragment remained intact, while the mutant allele-derived 370-bp fragment was digested into two fragments (220 and 150 bp). Migrating positions of the size marker DNA are shown in bp at left sides.

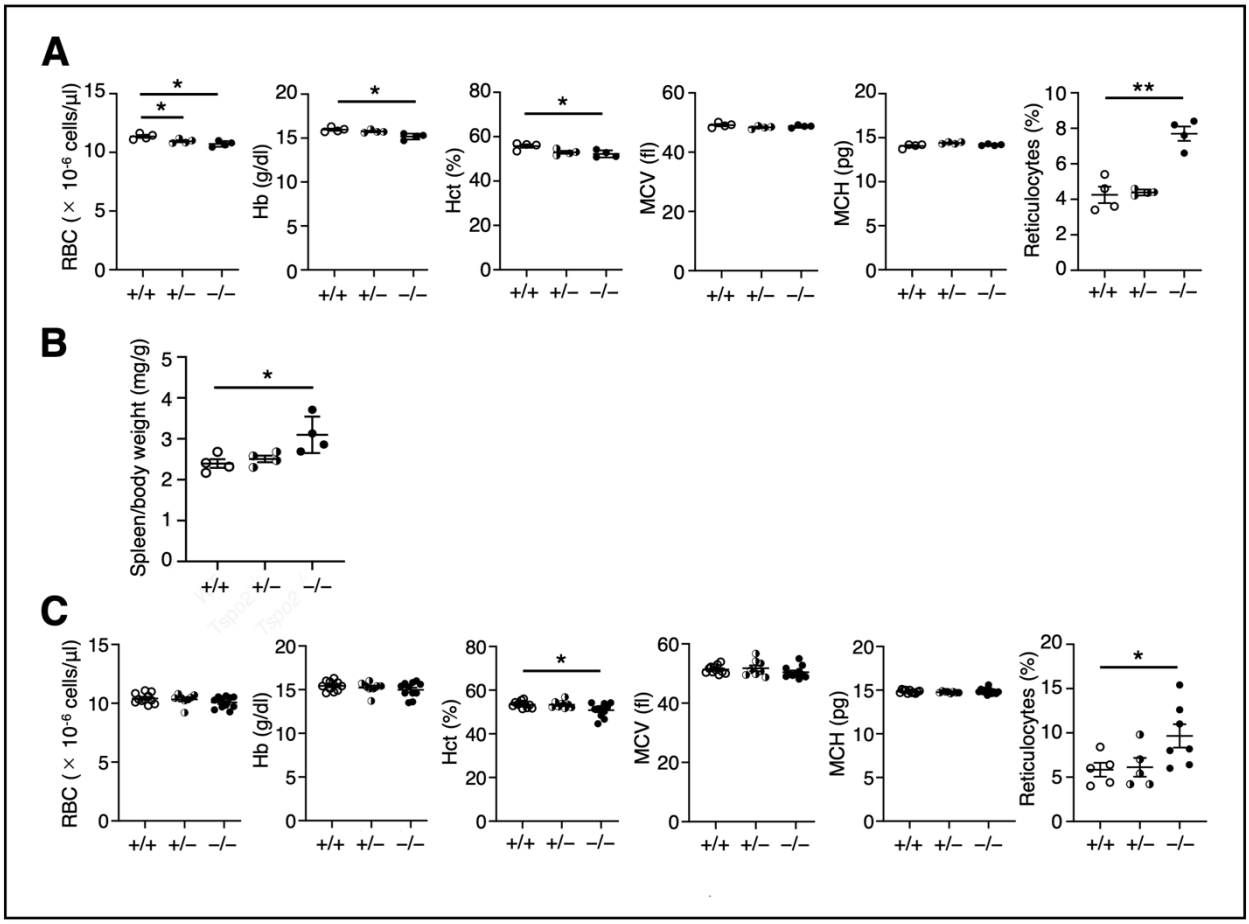



**Figure 2. Red blood cell phenotypes in *Tspo2*$^{-/-}$ mice**

**A.** RBC counts (*RBC*), hemoglobin concentration (*Hb*), hematocrit (*Hct*), mean corpuscular volume (*MCV*), mean corpuscular hemoglobin (*MCH*), and reticulocyte counts (*Reticulocytes*) in peripheral blood of 20-week-old *Tspo2*$^{+/+}$ (+/+, n = 4), *Tspo2*$^{+/-}$ (+/−, n = 4), and *Tspo2*$^{-/-}$ (−/−, n = 4) mice are shown. Data are expressed as the means ± S.E.M., **P* < 0.05, ***P* < 0.01. **B.** Spleen sizes of the mice in **A** are shown in the weight against the total body weight and expressed as the means ± S.E.M., **P* < 0.05. **C.** Hematological parameters are shown for *Tspo2*$^{+/+}$ (+/+, n = 11), *Tspo2*$^{+/-}$ (+/−, n = 8), and *Tspo2*$^{-/-}$ (−/−, n = 11) mice at 6~8 weeks of age are shown. Sample numbers for *Reticulocytes* are 5, 5, and 7 for +/+, +/−, and −/−, respectively. Data are expressed as the means ± S.E.M. **P* < 0.05.

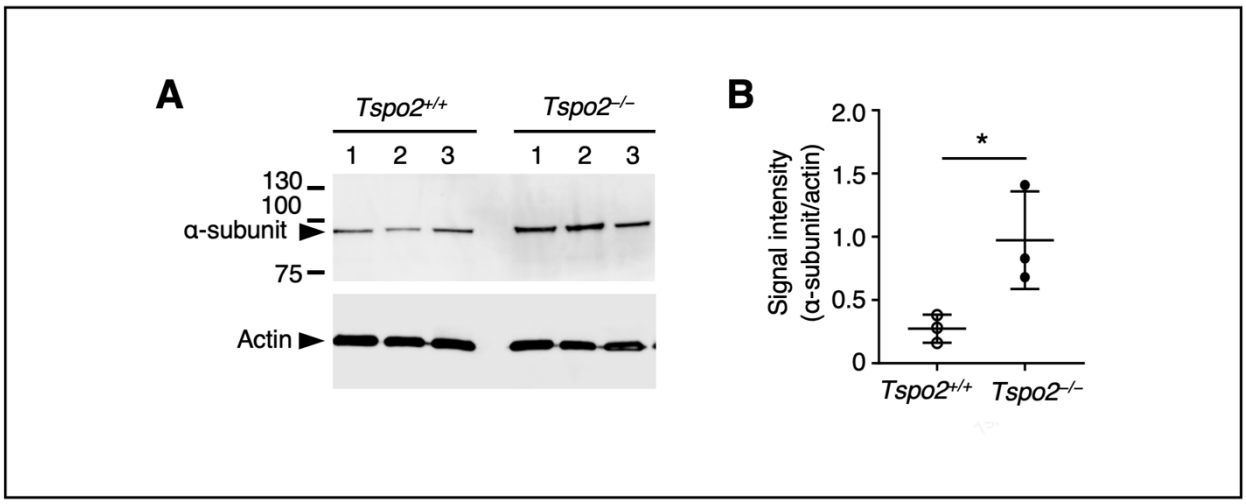



**Figure 3. Increased red cell membrane Na,K-ATPase contents in *Tspo2*$^{-/-}$ mice.**

**A.** Na,K-ATPase α-subunit contents in RBC membranes prepared from peripheral blood of *Tspo2*$^{+/+}$ (n = 3) and *Tspo2*$^{-/-}$ (n = 3) mice were analyzed by SDS-PAGE followed by immunoblotting as described previously (Inaba and Maede, 1986). The top half of the blot was probed with an antibody to Na,K-ATPase α-subunit and the bottom half of the blot was probed with an anti-β-actin antibody to detect β-actin for the internal control. Each lane contained 25 μg of RBC membrane proteins. **B.** The abundance of α-subunit relative to actin determined by densitometric scanning was 0.27 ± 0.11 (mean ± S.D., n = 3) in *Tspo2*$^{+/+}$ mice and 0.97 ± 0.39 (mean ± S.D., n = 3) in *Tspo2*$^{-/-}$ mice, respectively (*$P < 0.05$).

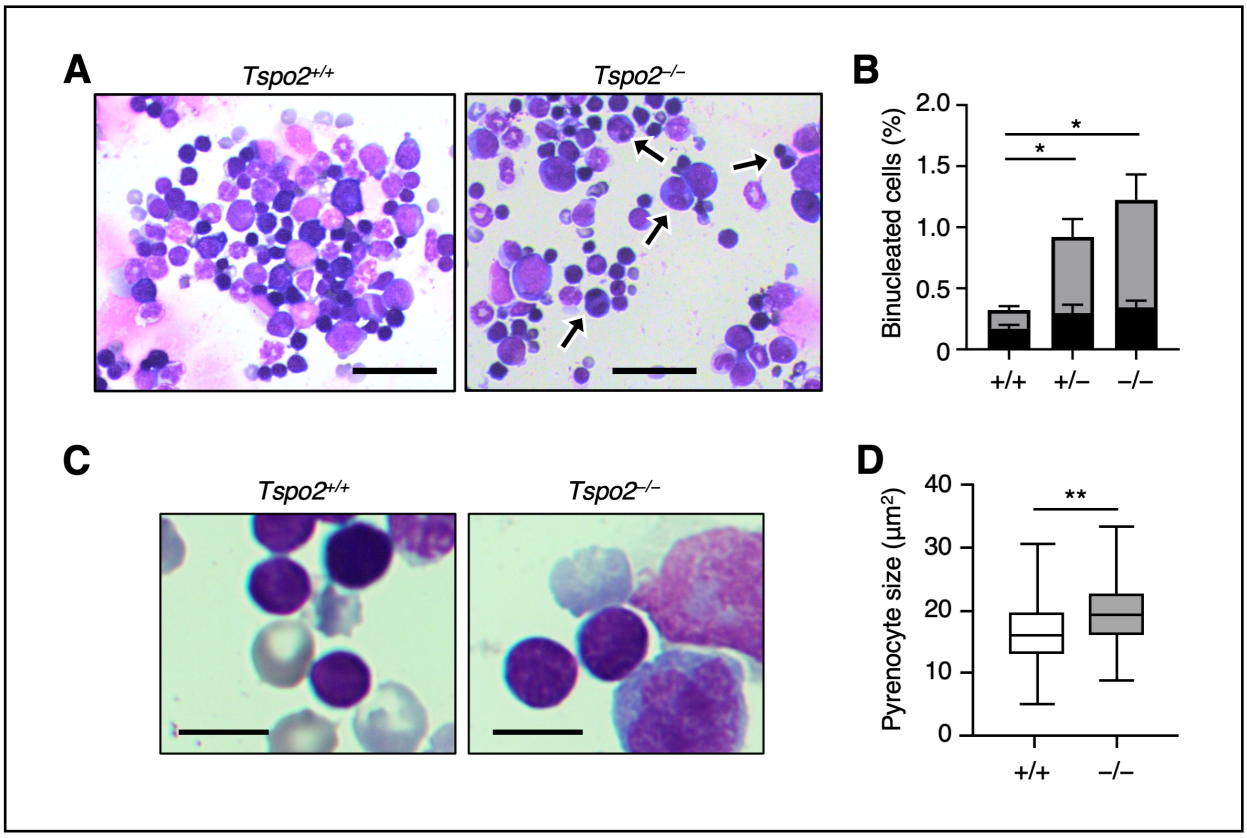



**Figure 4. Morphological phenotypes of BM-derived erythroid cells in *Tspo2*$^{-/-}$ mice.**

**A.** Wright-Giemsa-stained BM aspirates from 20-week-old *Tspo2*$^{+/+}$ (*Tspo2*$^{+/+}$) and *Tspo2*$^{-/-}$ (*Tspo2*$^{-/-}$) mice showed increased numbers of binucleated erythroblasts at various stages (*arrows*) in *Tspo2*$^{-/-}$ mice. Bars, 50 μm. **B.** The relative abundance of binucleated erythroblasts in *Tspo2*$^{+/+}$ (+/+, n = 4), *Tspo2*$^{+/-}$ (+/−, n = 4), and *Tspo2*$^{-/-}$ (−/−, n = 4) mice are presented as the means ± S.E.M. Gray and black columns indicate the abundance of polychromatic and orthochromatic erythroblasts or basophilic erythroblasts, respectively (*$P < 0.05$). **C.** Wright-Giemsa-stained enucleating erythroblasts in BM aspirates from 20-week-old *Tspo2*$^{+/+}$ and *Tspo2*$^{-/-}$ mice. Bars, 10 μm. **D.** The sizes of extruded nuclei (pyrenocytes) in *C* were analyzed as areas in μm$^2$. Data are expressed as box plots with whiskers from minimum to maximum, n = 200, **$P < 0.01$.

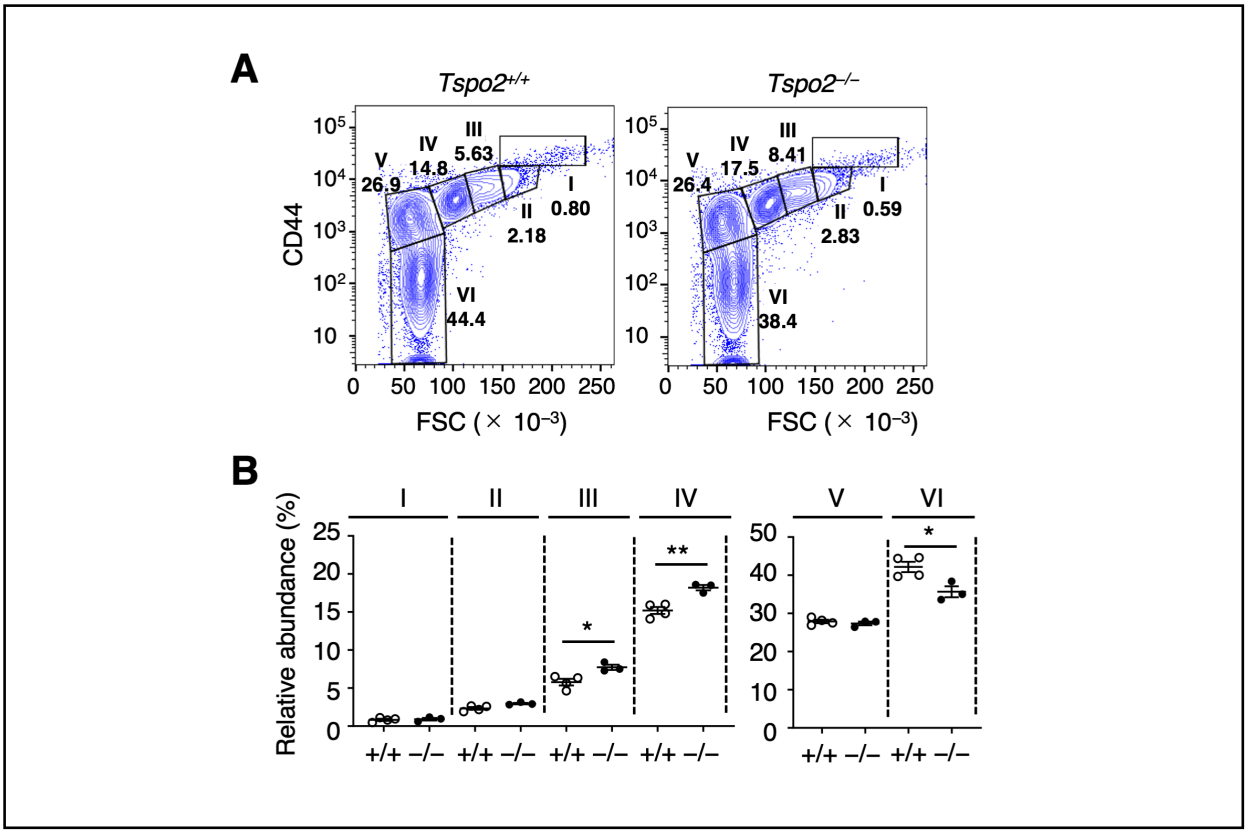



**Figure 5. CD44 expression in BM-derived erythroid cells from *Tspo2*$^{-/-}$ mice.**

**A.** BM-derived TER119-positive erythroid cells from 20-week-old *Tspo2*$^{+/+}$ (+/+, n = 3) and *Tspo2*$^{-/-}$ (−/−, n = 3) mice were analyzed for their CD44 expression (*CD44*) together with forward scatter (*FSC*) by flow cytometry as reported previously (Chen et al., 2009; Liu et al., 2015). **B.** Relative abundance of the cells in populations I~VI shown in *A*. **P* < 0.05, ***P* < 0.01.

## 2. Erythroid cell maturation and proliferation in *Tspo2* knockout cell line

To further clarify the effect of the TSPO2 defect on terminal erythropoiesis, *Tspo2*-deficient cell clones of MEDEP-BRC5 cells (*Tspo2*$^{-/-}$ MEDEP cells) were created. MEDEP cells showed characteristics of proerythroblasts or CFU-E (Hiroyama et al., 2008) and represented spaciotemporal changes in terminal differentiation very similar to those of primary mouse erythroid cells (Gautier et al., 2020). Consequent to a successive selection and cloning, two independent clones of *Tspo2*$^{-/-}$ MEDEP cells, clones KO13 and KO26, were obtained. Since clones KO13 and KO26 showed similar impairments in cell proliferation and hemoglobinization, further detailed studies were carried out using the clone KO13.

*Tspo2*$^{-/-}$ MEDEP cells revealed reduced *Tspo2* mRNA expression compared to the control MEDEP cells (Fig. 6A). *Tspo2*$^{-/-}$ cells showed a marked reduction in cell proliferation (Fig. 6B) and a significant increase in numbers of binucleated and multinucleated cells (Fig. 6C) compared to the control cells. An increase in annexin V-positive apoptotic cells by 33% compared to control cells was also documented in *Tspo2*$^{-/-}$ cells (Fig. 6D). Cell cycle analysis demonstrated that these defects in *Tspo2*$^{-/-}$ cells were accompanied by an arrest at G2/M stage as demonstrated by the cell number in G2/M population that was increased by 39% compared to control cells (Figs. 6E and 6F).

Moreover, while staining of the cells with filipin III and Nile Red revealed abundant cytoplasmic signals of free cholesterol and cholesteryl esters (CEs), respectively, in control cells, both filipin and Nile Red signals in *Tspo2*$^{-/-}$ MEDEP cells showed profound reduction in staining. However, NBD-cholesterol uptake in *Tspo2*$^{-/-}$ MEDEP cells was apparently comparable to that in the control cells (Fig. 7). These data indicate that *Tspo2*$^{-/-}$ MEDEP cells had a decreased ability to regulate both free and esterified cholesterol, despite their ability to incorporate extracellular cholesterol into the cells.

Then, the effects of the TSPO2 defect on erythropoiesis was examined in MEDEP cells after induction with erythropoietin. The control cell numbers increased by 8-fold at 48 hours, while *Tspo2*$^{-/-}$ MEDEP cells showed only a 4.5-fold increase (Fig. 8A). During this period, both control and *Tspo2*$^{-/-}$ MEDEP cells matured progressively and underwent enucleation as shown in Fig. 8B. At 48 hours of incubation, the control culture comprised mainly of the cells whose morphology resembled that of orthochromatic erythroblasts, enucleated reticulocytes, and pyrenocytes. In contrast, cells in *Tspo2*$^{-/-}$ culture were heterogeneous in appearance, containing cells ranging from basophilic to orthochromatic erythroblasts with considerably increased numbers of binucleated and apoptotic cells (Fig. 8B). There were much fewer enucleating cells (lower enucleation rate) in *Tspo2*$^{-/-}$ cell culture compared to the control culture (10.0% ± 1.3% *vs.* 45.7% ± 2.4%, means ± S.D., n =3, Fig. 8C). The size of expelled pyrenocyte in *Tspo2*$^{-/-}$ cell culture was significantly larger than that in control cell culture (Figs. 8D and 8E).

Maturing *Tspo2*$^{-/-}$ MEDEP cells also showed a remarkable reduction in hemoglobin content that was less than 60% of that in control cells at 48 hours (Figs. 9A and 9B). However, there was no major difference between *Tspo2*$^{-/-}$ and control cells through the maturation process in the mRNA expression levels of the genes relevant to hemoglobin synthesis such as *Hba*, *Hbb*, *TfR*, and *Alas2*, as well as several erythroid genes essential for the terminal erythropoiesis including *Gata1*, *Klf1*, *Setd8*, and *Slc4a1* (Fig. 10).

Furthermore, remarkable differences were found in the expression of phenotypic markers of erythropoiesis following *Tspo2* knockout (Figs. 11A and 11B). Before induction into maturation, the major population of control and *Tspo2*$^{-/-}$ MEDEP cells had high CD71 and low TER119 expression levels (CD71$^{high}$/TER119$^{low}$). Control cells progressed into CD71$^{high}$/TER119$^{high}$ at 24 hours and a subpopulation of cells matured into CD71$^{low}$/TER119$^{high}$

cells at 48 hours after induction. In contrast, significant numbers of *Tspo2*$^{-/-}$ cells remained in CD71$^{high}$/TER119$^{low}$ population at 24 hours and in CD71$^{high}$/TER119$^{high}$ population without increase of cells in CD71$^{low}$/TER119$^{high}$ compartment after 48 hours. At 72 hours, although both control and *Tspo2*$^{-/-}$ cells showed a further reduction in CD71 expression, the number of CD71$^{low}$/TER119$^{high}$ population was retained at a low level in *Tspo2*$^{-/-}$ cells.

Moreover, the median fluorescent intensity (MFI) of CD44 in *Tspo2*$^{-/-}$ cells, that was slightly higher than that in control at the onset of culture, remained at higher expression levels compared to control cells at 48 hours, and finally decreased to the levels compatible with control cells at 72 hours (Fig. 12A). Cells could be divided into two populations at 48 hours according to their sizes (fraction P1 and others, Fig. 12B). The population of more mature cells with smaller sizes and lower levels of CD44 (P1 fraction) in *Tspo2*$^{-/-}$ cells was less abundant compared to that in control cells (29.3% ± 2.6% *vs.* 43.6% ± 1.0%, mean ± S.D., n =3, Fig. 12C). In addition, the MFI of CD44 in P1 fraction of *Tspo2*$^{-/-}$ cells was significantly higher than that in control cells (840 ± 95 *vs.* 323 ± 62, mean ± S.D., n =3, Fig. 12D). These data indicate that morphologic and phenotypic maturation of *Tspo2*$^{-/-}$ MEDEP cells is markedly delayed.

These delays in morphologic maturation, hemoglobinization, and changes in phenotypic markers suggest that *Tspo2*$^{-/-}$ cells cycled slower to mature into reticulocytes. To test this, the cells were labeled with the tracer dye CellTrace Violet and analyzed for the reduction in tracer dye intensities. The profile for the reduction in tracer dye intensities and the MFI values obtained indicated that *Tspo2*$^{-/-}$ cells were slightly lagged behind the control cells in cell division (Figs. 13A and 13B). Assuming a reduction in the tracer dye MFI by the factor 2 with each division, the control cells had an average of 5.6 cell divisions after 48 hours of induction when there were many enucleating cells. Notably, there was an average of 0.7 fewer cell

divisions in *Tspo2*$^{-/-}$ cells at 48 hours (Fig. 13C). Fewer numbers of cell divisions were also apparent at 12, 36, and 24 hours, indicating that there were cumulative delays with roughly an average of 2-hour time-lag for every cell divisions. This assumption is compatible with lower rates of enucleation in *Tspo2*$^{-/-}$ cells described above. In *Tspo2*$^{-/-}$ cells, therefore, the alteration in the cell-cycle progression but not the number of cell divisions is implicated in the delayed terminal maturation.

Integrating the findings from MEDEP cells and *Tspo2*$^{-/-}$ mice implies that the *Tspo2* defect causes the delays in multifaceted events during terminal erythroid differentiation and cell-cycle progression and strongly supports that the failures in maturation and cytokinesis of HK dog erythroblasts are attributable to the TSPO2 defect.

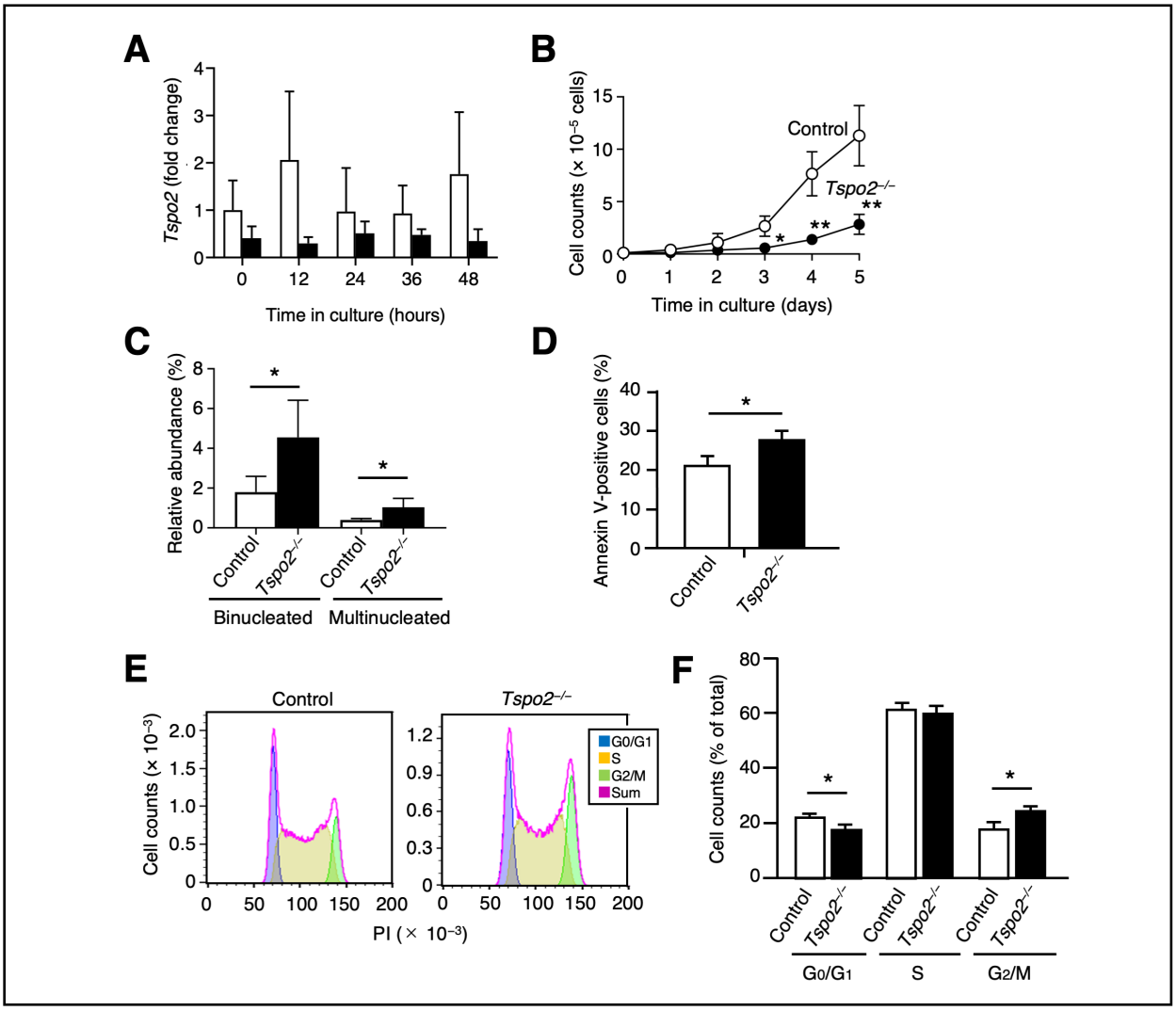



**Figure 6. Cellular phenotypes in self-renewal of *Tspo2* knockout MEDEP cells.**

**A.** The relative abundance of *Tspo2* mRNA expression in control (*Control*) and *Tspo2*$^{-/-}$ (*Tspo2*$^{-/-}$) MEDEP cells were analyzed by qRT-PCR. The data are normalized by the expression level of *Gapdh* and expressed as the means ± S.D. (n = 3) relative to that in control MEDEP cells at time 0. *Tspo2* mRNA levels in *Tspo2*$^{-/-}$ cells were lower than those in control cells throughout the incubation period. **B.** Proliferation of control and *Tspo2*$^{-/-}$cells in cell culture in the absence of erythropoietin. Data are shown as the means ± S.D. (n = 4). **P* < 0.05, ***P* < 0.01. **C.** After 4 days in culture, cytospin smears were prepared and the cells were stained with Wright-Giemsa. The numbers of cells with abnormal morphology including binucleated and multinucleated cells were counted. Data are expressed as the means ± S.D. (n = 4). **P* < 0.05. **D.** At day 3 in culture, the relative abundance of annexin V-positive apoptotic cells were determined by flow cytometry. Data are expressed as the means ± S.D. (n = 7). **P* < 0.05. **E.** Representative histograms of cell cycle analysis for the control and *Tspo2*$^{-/-}$ cells. Cells were

collected on day 3, stained with PI, and analyzed by flow cytometry. **F.** Relative abundance of $G_0/G_1$, S, and $G_2$/M phases were determined using FlowJo software. Data are expressed as the means ± S.D. (n = 6). *$P < 0.05$.

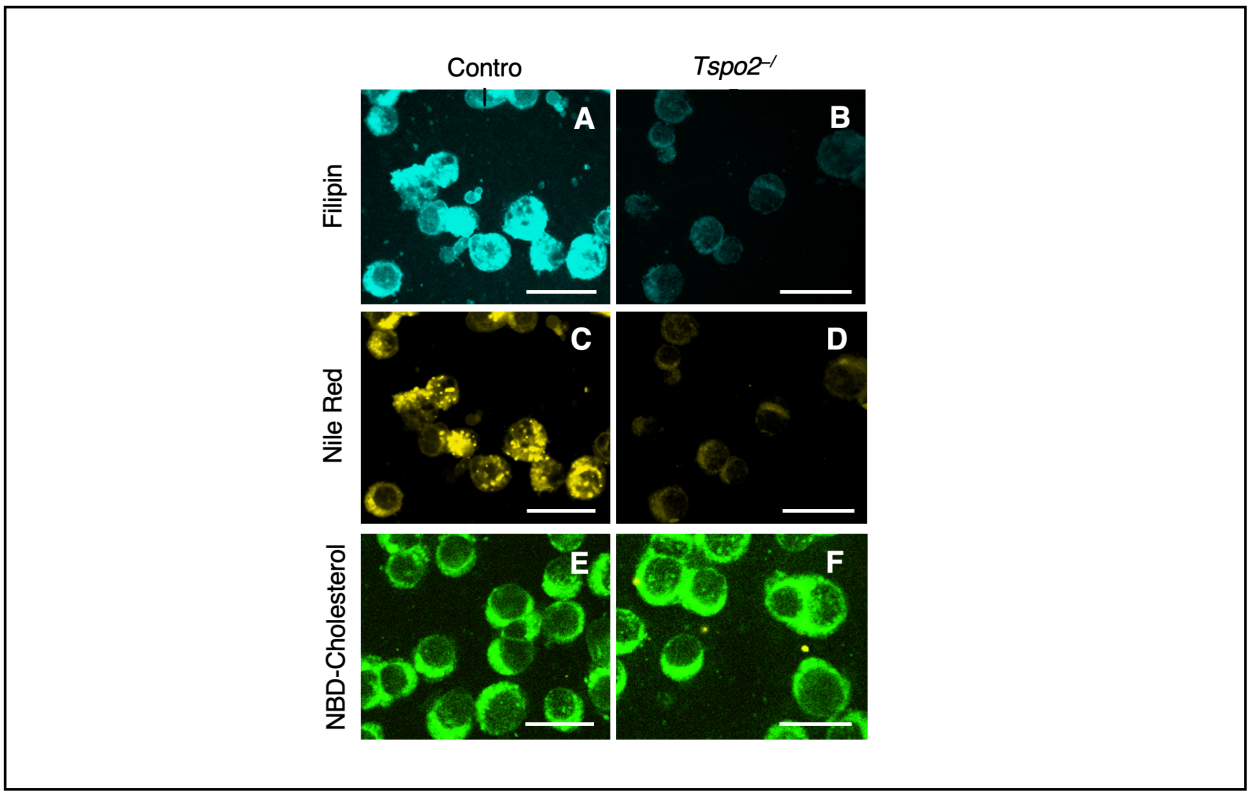



**Figure 7. Reduction of intracellular cholesterol in *Tspo2*$^{-/-}$ MEDEP cells**

Control and *Tspo2*$^{-/-}$ cells were counterstained with filipin III *(Filipin)* and Nile Red *(Nile Red)* to detect unesterified cholesterol and cholesteryl esters (CEs), respectively. NBD-cholesterol uptake into the cells after 10-minute incubation *(NBD-cholesterol)* is also shown. Representatives from four independent experiments are shown. Bars, 20 µm.

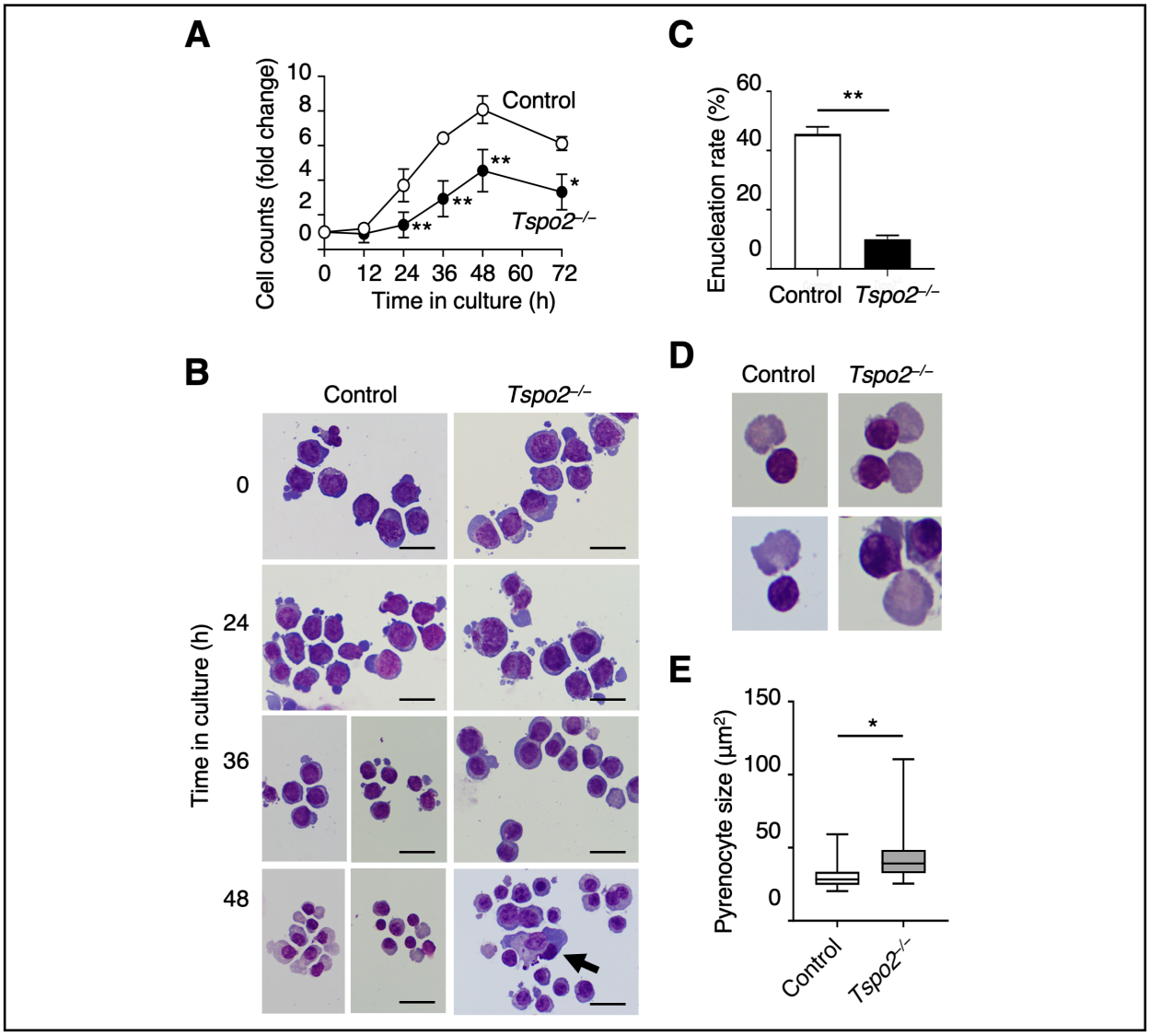



**Figure 8. Impaired proliferation and abnormal morphology in maturing *Tspo2* knockout MEDEP cells.**

**A.** Proliferation of control (*Control*) and *Tspo2*$^{-/-}$ (*Tspo2*$^{-/-}$) MEDEP cells in culture for 72 hours after induction of terminal erythroid differentiation with erythropoietin. The changes in cell counts are shown in multiples of the initial cell counts and are expressed as the means ± S.D. (n = 3). **P* < 0.05, ***P* < 0.01. **B.** At the indicated time of incubation, cytospin smears were prepared and stained with Wright-Giemsa. *Tspo2*$^{-/-}$ cell culture contained increased numbers of binucleated cells and the cells with apoptotic features (*arrow*). Bars, 20 µm. **C.** At 48 hours in culture, enucleating cells in the control and *Tspo2*$^{-/-}$ cell cultures were counted and their relative abundance against total cells (200 cells) are shown as the enucleation rate. Data are expressed as the means ± S.D. (n = 3). ***P* < 0.01. **D** and **E**. Enucleating cells in the control

and *Tspo2*$^{-/-}$ cell cultures (n = 50 for each, representatives are shown in **D**) were analyzed for the size of extruded pyrenocytes. *$P < 0.05$.

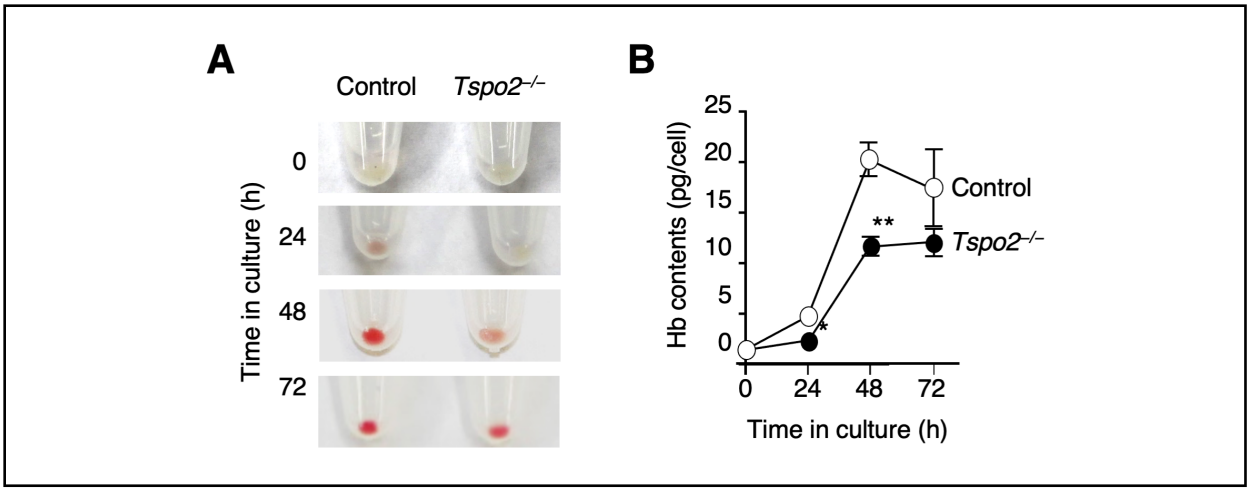



**Figure 9. Delayed hemoglobinization in *Tspo2* knockout MEDEP cells.**

Control (*Control* or *open circle*) and *Tspo2*$^{-/-}$ (*Tspo2*$^{-/-}$ or *closed circle*) MEDEP cells were incubated as described in the legend for Fig. 8. Cells were collected at the indicated time and the color of cell pellets (**A**) and hemoglobin contents (**B**) were examined. In **B**, data are expressed as the means ± S.D. (n = 3). **P* < 0.05, ***P* < 0.01.

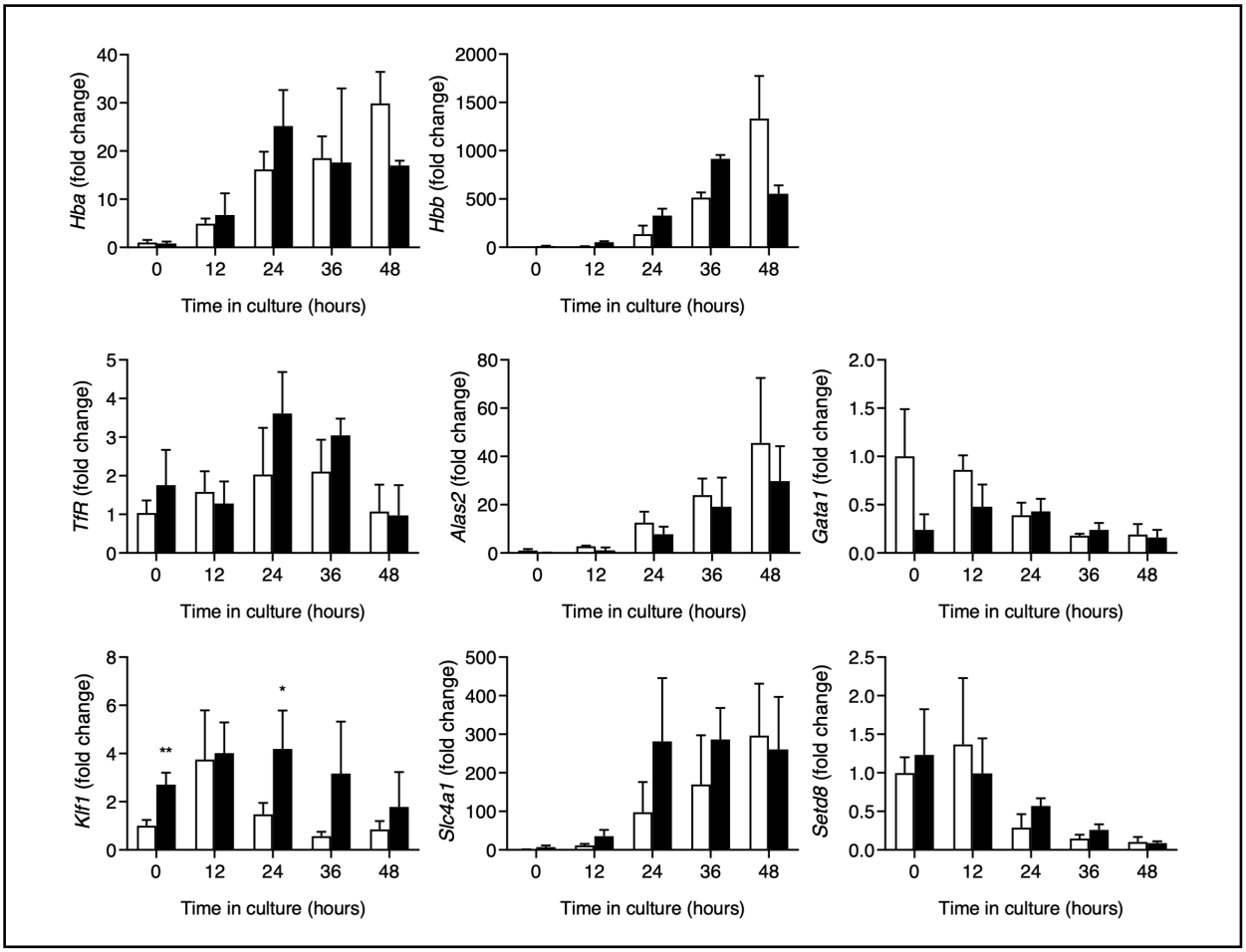



**Figure 10. Expression of erythroid-specific genes in maturing MEDEP cells**

The relative abundance of mRNAs of some late erythroblast-specific genes in maturing control (*white bars*) and *Tspo2*$^{-/-}$ cells (*black bars*) were analyzed by qRT-PCR. The genes examined include *Hba* (α-globin), *Hbb* (β-globin), *TfR* (transferrin receptor), *Alas2* (5'-aminolevulinate synthase 2), *Gata1*, *Klf1*, *Slc4a1* (anion exchanger 1, band 3), and *Setd8* (histone methyltransferase). The data are normalized by the expression level of *Gapdh* and expressed as the means ± S.D. (n = 3) relative to that in control MEDEP cells at time 0. There were no major differences between control and *Tspo2*$^{-/-}$ cells in mRNA expressions of these genes through incubation period except that higher expression of *Klf1* was apparent in *Tspo2*$^{-/-}$ cells at several time points. **P* < 0.05, ***P* < 0.01.

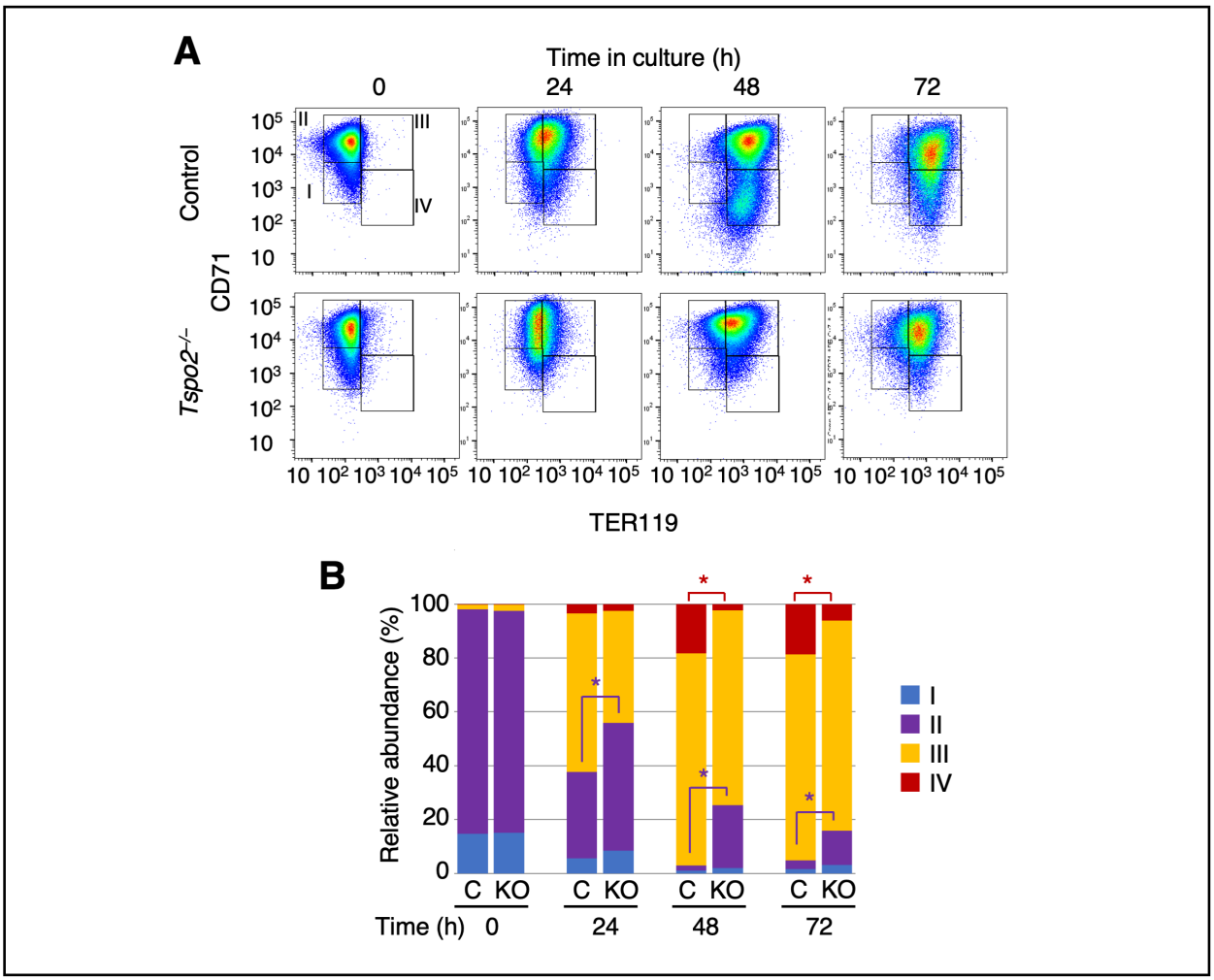



**Figure 11. Impaired maturation-associated change in CD71/TER119 expression in *Tspo2* knockout MEDEP cells.**

**A.** Representative data of flow cytometric analyses for CD71 *vs.* TER119 in maturing control (*Control*) and *Tspo2*$^{-/-}$ (*Tspo2*$^{-/-}$) MEDEP cells at the indicated time of incubation are shown. **B.** The cells are divided into four fractions (*I~IV*) as indicated in **A**, and the relative abundance (%) of the cells in each fraction at different time points are shown. Data are expressed as the mean values (n = 5). S.D. values are not shown for simplification. **P* < 0.05. Control and *Tspo2*$^{-/-}$ cells are indicated as *C* and *KO*, respectively.

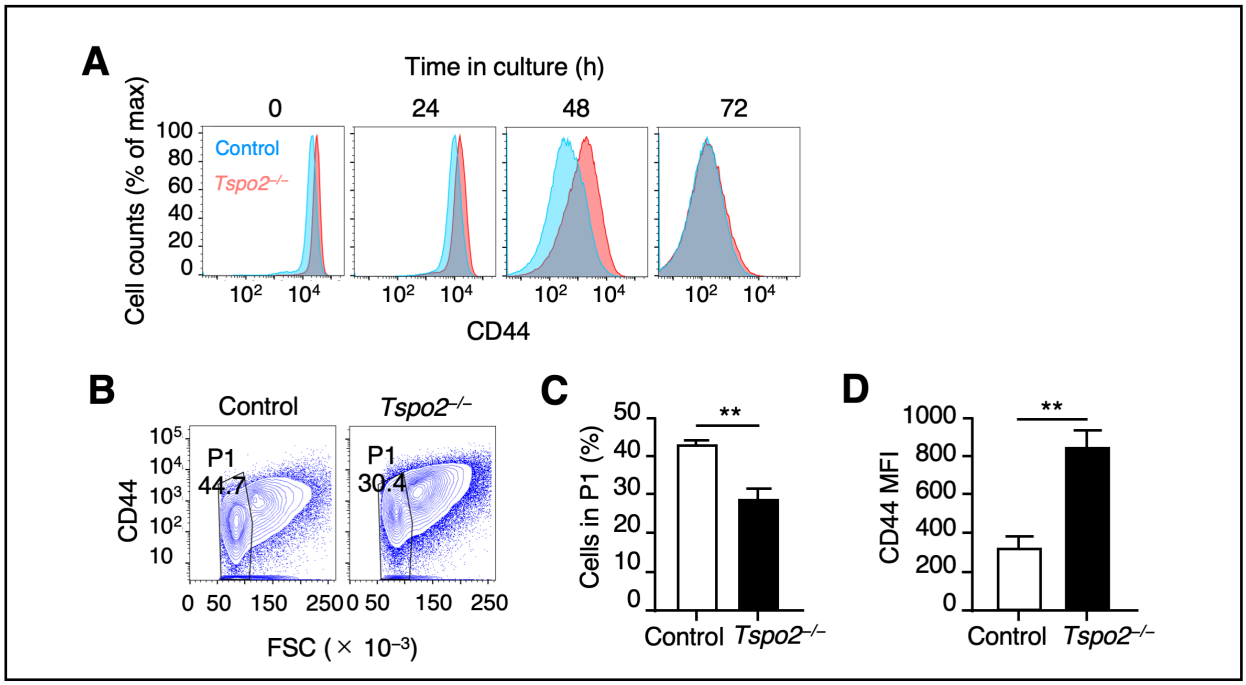



**Figure 12. Impaired maturation-associated changes of CD44 expression in *Tspo2* knockout MEDEP cells.**

**A.** Representative data from 3 independent flow cytometric analyses for cell surface CD44 *vs.* cell counts in maturing control (*Control*) and *Tspo2*$^{-/-}$ (*Tspo2*$^{-/-}$) cells at the indicated time in culture are shown. **B.** Representative histograms for CD44 *vs*. FSC in maturing control (*Control*) and *Tspo2*$^{-/-}$ (*Tspo2*$^{-/-}$) cells at 48 hours. **C** and **D**. P1 fractions from control and *Tspo2*$^{-/-}$ cells shown in **B** were analyzed for the abundance relative to the total numbers of cells (**C**) and MFI of CD44 (**D**). Data are expressed as the means ± S.D. (n = 3). $^{**}P < 0.01$.

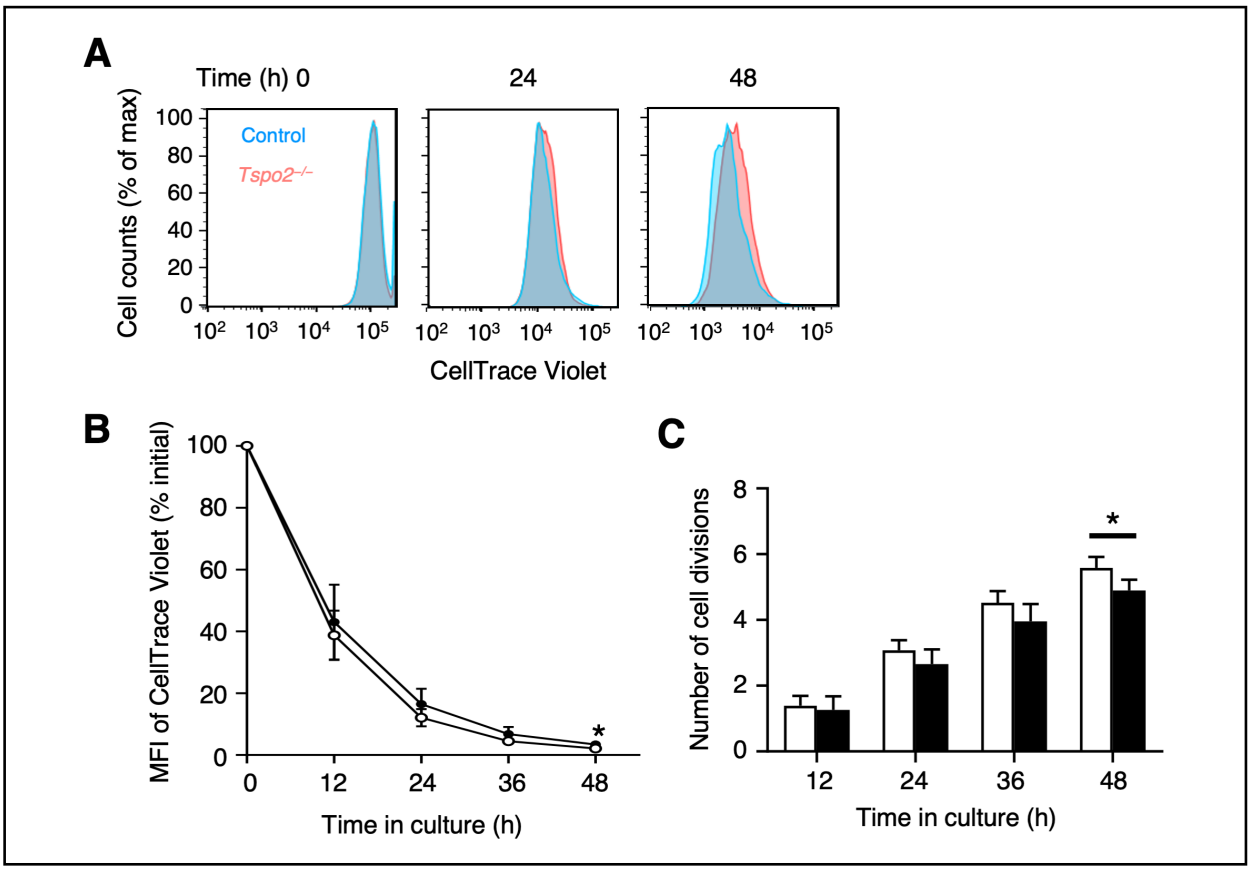



**Figure 13. Delayed cell division in *Tspo2* knockout MEDEP cells.**

**A.** Maturing control (*Control*) and *Tspo2*$^{-/-}$ (*Tspo2*$^{-/-}$) cells were labeled with a tracer dye CellTrace Violet and chased for the decline of incorporated dye by flow cytometry. A representative data for the fluorescent intensity *vs.* cell counts from 4 independent analyses is shown. **B.** Decline profile of the MIF obtained from 4 independent analysis. Data are expressed as the means ± S.D. (n = 4). **P* < 0.05. **C.** The number of cell divisions of maturing control (*white bars*) and *Tspo2*$^{-/-}$ (*black bars*) cells was determined at the indicated time periods in culture as described previously (Sankaran et al., 2012) and are expressed as the means ± S.D. (n = 4). **P* < 0.05.

# Discussion

The findings from the present study revealed an important *in vivo* functional role for TSPO2 in both maturation and proliferation of late stage erythroblasts. Similar defects in cell proliferation are also noted in the self-renewal of *Tspo2*$^{-/-}$ MEDEP cells. The noted defects both in *in vivo* and *in vitro* mouse models are prominent in basophilic, polychromatic, and orthochromatic erythroblasts, the erythroid differentiation stages at which TSPO2 is highly expressed (Fan et al., 2009) and consistent with the erythroid phenotypes observed in HK dogs (Kiatpakdee et al., in press). The present findings indicate that TSPO2 is essential for maturation and proliferation of erythroblasts to efficiently produce normal RBCs (Fig. 14 illustrates the summary of the present study). Considering the reduced cell proliferation and hemoglobinization in *Tspo2*$^{-/-}$ MEDEP cells and anemic phenotypes in *Tspo2*$^{-/-}$ mice, the TSPO2 defect may reduce the efficiency of RBC production by ~50%. The finding that key erythroid genes in terminal erythropoiesis such as *Gata1*, *Klf1*, *TfR*, *Alas2*, *Hba*, *Hbb*, and *Setd8* (Dizierzak and Philipsen, 2013; Malik et al., 2015; Malik et al., 2017; Papayannopoulou and Migliaccio, 2017) are expressed at similar levels in control and *Tspo2*$^{-/-}$ MEDEP cells implies that TSPO2-deficient erythroblasts are able to execute principal aspects of the terminal erythropoiesis program. As there is no reduction in the number of cell division prior to enucleation in TSPO2-deficient cells, perturbed maturation and cell proliferation due to the TSPO2 defects are most likely attributable to a delayed cell-cycle progression associated with impaired cytokinesis. Although TSPO2 has originally been suggested to have a role in cholesterol redistribution in erythroblasts (Fan et al., 2009), the functional sequela of this observation was not defined. The findings of the present study have implicated a major functional role for TSPO2 in erythropoiesis.

Since cholesterol is an essential component of cell membranes, proliferating cells have highly active cholesterol metabolism. Indeed, frequent hypocholesterolemia in patients with chronic anemias (Shalev et al., 2007) and acute leukemia (Vitols et al., 1985) suggests increased demand for cholesterol in proliferation of hematopoietic cells. In cytokinesis, cholesterol is essential for vesicular trafficking to form a membrane domain at the cleavage furrow ingression (Ng et al., 2005; Montagnac et al., 2008) and mid-body tubules, a novel membrane-bound intercellular bridge (Kettle et al., 2015). Lack of availability of cholesterol therefore causes cells to spend a prolonged period in cytokinesis and an increase in multinucleation (Kettle et al., 2015). Furthermore, earlier studies had demonstrated that cholesterol starvation in human leukemia HL-60 cells induces the inhibition of cell proliferation and cell-cycle arrest selectively in G2/M phase and the consequent formation of multinucleated polyploid cells (Martinez-Botas et al., 1999; Fernández et al., 2004; Fernández et al., 2005). The phenotypes observed in several distinct models in our study are compatible with such reported manifestations and confirm that cholesterol is essential for cell division and cell-cycle progression in hematopoiesis (Fig. 14). Notably, a profound reduction in cholesterol content in *Tspo2*$^{-/-}$ MEDEP cells strongly suggests that the *Tspo2* aberration causes cholesterol depletion in maturing erythroblasts. Taken together, our findings with both *in vivo* and *in vitro* models imply that restricted availability or depletion of cholesterol is most likely the primary cause for the impairments in cell-cycle progression and cytokinesis due to the TSPO2 defect.

Our previous work (Kiatpakdee et al., in press) also demonstrates that the expression of cTSPO2 in K562 cells causes cholesterol accumulation in the endoplasmic reticulum (ER). In general, the ER receives cholesterol from the plasma membrane, other intracellular organelles including the endocytic recycling compartment and the *trans*-Golgi network, or via *de novo* synthesis, and then recycles it back to the plasma membrane through several distinct pathways (Mukherjee et al., 1998; Maxfield and Tabas, 2005; Ikonen, 2008; Rone et al., 2009). Excess

cholesterol is esterified and stored as CEs in lipid droplets and is released again after esterification hydrolysis, when needed. Interestingly, both of these conversions occur in the ER (Maxfield and Tabas, 2005; Zhang et al., 2017) and it is suggested that excess cholesterol is exported from the ER rather than being esterified (Zhang et al., 2017). As the appearance of TSPO2 parallels with downregulation of *de novo* synthesis of cholesterol during erythroblast maturation (Fan et al., 2009), we suggest that TSPO2 participates in redistribution, including accumulation of free cholesterol in the ER, from internal or extracellular resources to efficiently provide cholesterol to the plasma membrane. Our finding of the decreased cholesterol availability in *Tspo2*$^{-/-}$ MEDEP cells, as well as a reduction in CEs and a simultaneous increase in free cholesterol in K562 cells expressing wild-type cTSPO2 (Kiatpakdee et al., in press), supports this thesis and suggests that lipid droplets can be the intracellular source of cholesterol. Moreover, this assumption is consistent with a role for cholesterol-enriched membrane domain that has been implicated in vesicular trafficking and cytokinesis (Ng et al., 2005; Montagnac et al., 2008; Kettle et al., 2015). It is also compatible with the requirement of cholesterol in enucleation that involves endocytic vesicular trafficking, Rac GTPase-dependent assembly of lipid rafts, and coalescence of lipid rafts between reticulocyte and pyrenocyte (Keerthivasan et al, 2010; Konstantinidis et al., 2012). On the other hand, cholesterol levels in the ER have been shown to selectively regulate secretory protein trafficking through the COPII vesicular transport pathway (Espenshade et al., 2002; Runz et al., 2006; Bonnon et al., 2010). Accordingly, a possible regulation of cholesterol levels in the ER by TSPO2 may also affect the ER-to-Golgi transport and the plasma membrane expression of some membrane proteins during erythropoiesis.

Thus, the TSPO2 defects result in immature RBC phenotypes as demonstrated in HK dog RBCs (Maede and Inaba, 1987; Inaba and Maede, 1989; Komatsu et al., 2010), presumably due to the delayed and incomplete maturation. The HK RBC trait in dogs is a recessive phenotype

that depends on the total loss of Na,K-ATPase in erythrocytes. However, the TSPO2 defects appear to have dominant effects in erythropoiesis as demonstrated by the erythroid phenotypes in the knockout mice, although they have modest RBC phenotypes (Maede et al., 1983; Inaba and Maede, 1986; Komatsu et al., 2010). One inconsistency in the present models is that TSPO2 defects result in a larger size of nascent reticulocytes in maturing MEDEP cells, while there was no significant difference in size of circulating RBCs in knockout mice. This discrepancy may be attributable to a further maturation of released reticulocytes by phagolysosome expulsion of organelles (Holm et al., 2002) and the plasma membrane remodeling (Lazarides and Moon, 1984; Hanspal and Palek, 1987; Mohandas and Gallagher, 2008). Indeed, HK erythrocytes possess no remnant organelles, and HK and LK reticulocytes exhibit similar changes in the membrane protein composition by proteolysis or exosome expulsion during maturation into erythrocytes (Inaba and Maede, 1986; Komatsu et al., 2010). Thus, TSPO2 is essential for survival and coordinated maturation and proliferation of erythroblasts, while it is dispensable in further maturation of the enucleate progeny.

Apart from the cholesterol-related function, TSPO2 has recently been reported to be involved in the membrane transport of a heme analogue protoporphyrin IX or ATP in human RBCs by forming a supramolecular complex with the voltage-dependent anion channel (VDAC) and adenine nucleotide transporter (ANT) (Marginedas-Freixa et al., 2016; Marginedas-Freixa et al., 2018). A mitochondrial paralogous protein TSPO also forms a complex with VDAC and ANT to mediate various mitochondrial functions, including cholesterol and porphyrin transport, generation of reactive oxygen species, and cell proliferation (Papadopoulos et al., 2006; Rupprecht et al., 2010). Further studies need to define whether TSPO2 is involved in the formation of a similar protein complex and its relevant membrane transport function in the ER in erythroblasts.

In conclusion, the present study has identified a regulatory role of TSPO2 on cell-cycle progression and cytokinesis in erythropoiesis. Although the precise mechanism remains to be fully defined, TSPO2 appears to play an essential role in maintaining cholesterol availability, leading to harmonized maturation and proliferation of late erythroblasts.

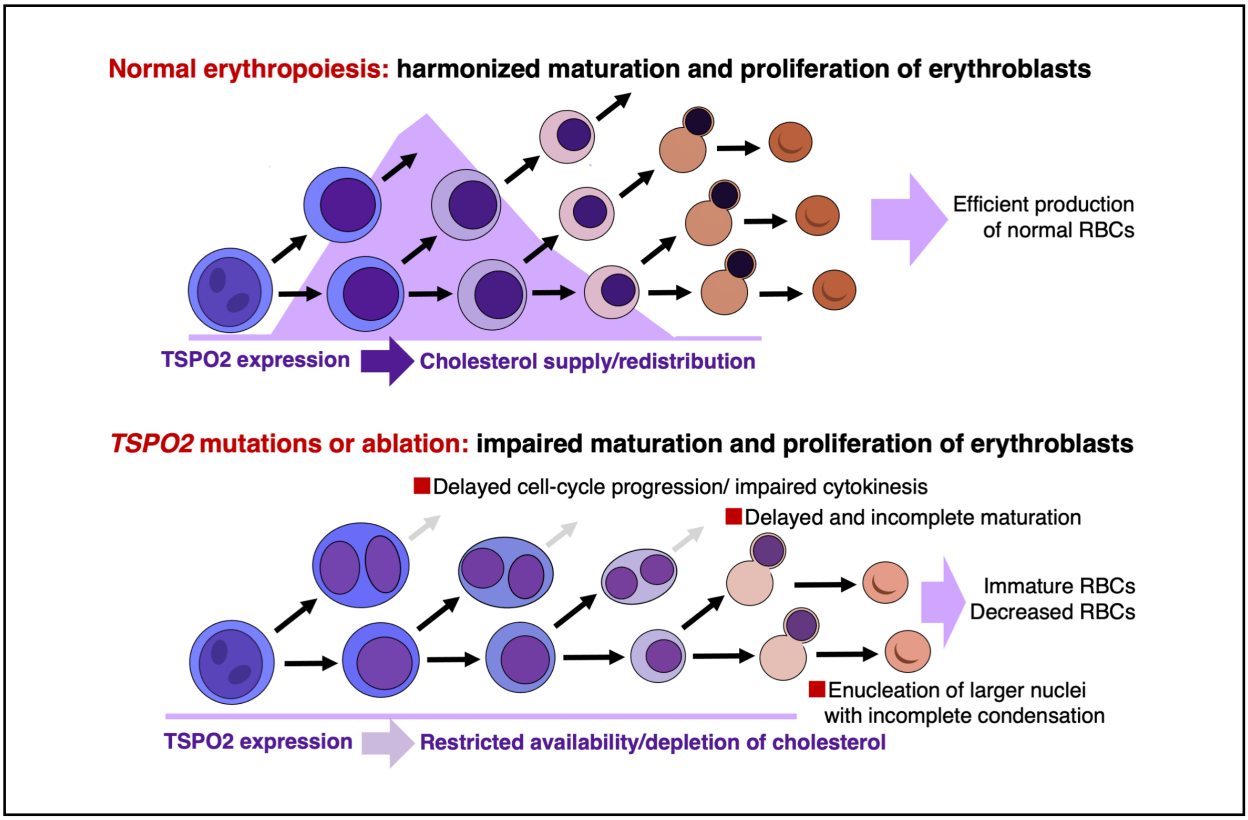



**Figure 14. TSPO2 plays essential roles in maturation and proliferation of late erythroblasts in erythropoiesis**

The summary of the present study is illustrated. The TSPO2 defect caused delays in cell-cycle progression and maturation of late-stage erythroblasts associated with cytokinesis failure and enucleation of larger nuclei with incomplete condensation, leading to inefficient production of RBCs with immature phenotypes. These findings demonstrate that TSPO2 is essential for coordinated maturation and proliferation of erythroblasts to effectively produce RBCs and suggest that TSPO2 supports cell-cycle progression and cytokinesis of erythroblasts possibly through regulating intracellular cholesterol availability.

# References


Azarashvili, T., Grachev, D., Krestinina, O., Evtodienko, Y., Yurkov, I., Papadopoulos, V., and Reiser, G. (2007) The peripheral-type benzodiazepine receptor is involved in control of $Ca^{2+}$-induced permeability transition pore opening in rat brain mitochondria. *Cell Calcium* **42**, 27–39.

Bonnon, C., Wendeler, M. W., Paccaud, J. P., and Hauri, H. P. (2010) Selective export of human GPI-anchored proteins from the endoplasmic reticulum. *J. Cell Sci.* **123**, 1705–1715.

Chan, P. C., Calabrese, V., and Theil, L. S. (1964). Species differences in the effect of sodium and potassium ions on the ATPase of erythrocyte membranes. *Biochim. Biophys. Acta* **79**, 424–426.

Chen, K., Liu, J., Heck, S., Chasis, J. A., An, X., and Mohandas, N. (2009) Resolving the distinct stages in erythroid differentiation based on dynamic changes in membrane protein expression during erythropoiesis. *Proc. Natl. Acad. Sci. U.S.A.* **106**, 17413–17418.

Cioe, L., McNab, A., Hubbell, H. R., Meo, P., Curtis, P., and Povera, G. (1981) Differential expression of the globin genes in human leukemia K562(S) cells induced to differentiate by hemin or butyric acid. *Cancer Res*. **41**, 237–243.

Cong, L., Ran, F. A., Cox, D., Lin, S., Barretto, R., Habib, N., and Zhang, F. (2013) Multiplex genome engineering using CRISPR/Cas systems. *Science* **339**, 819–823.

Dzierzak, E., and Philipsen, S. (2013) Erythropoiesis: development and differentiation. *Cold Spring Harb. Perspect. Med.* **3**, a011601.

Espenshade, P. J, Li, W. P., and Yabe, D. (2002) Sterol block binding of COPII proteins to SCAP, thereby controlling SCAP sorting in ER. *Proc. Natl. Acad. Sci. U.S.A.* **99**, 11694–11699.

Fan, J., Lindemann, P., Feuilloley, M. G. J., and Papadopoulos, V. (2012) Structural and functional evolution of the translocator protein (18 kDa). *Curr. Mol. Med*. **12**, 369–386.

Fan, J., Rone, M. B., and Papadopoulos, V. (2009) Translocator protein 2 is involved in cholesterol redistribution during erythropoiesis. *J. Biol. Chem*. **284**, 30484–30497.

Fernández, C., Lobo, M. D. V. T., Gómez-Coronado, D., and Lasunción, M. A. (2004) Cholesterol is essential for mitosis progression and its deficiency induces polyploid cell formation. *Exp. Cell Res.* **300**, 109–120.

Fernández, C., Martín, M., Gómez-Coronado, D., and Lasunción, M. A. (2005) Effects of distal cholesterol biosynthesis inhibitors on cell proliferation and cell cycle progression. *Lipid Res.* **46**, 920–929.

Gautier, E.-F., Leduc, M., Ladli, M., Schultz, V. P., Lefèvre, C., Boussaid, I., Fontenay, M., Lacombe, C., Verdier, F., Guillonneau, F., Hillyer, C. D., Mohandas, N., Gallagher, P. G., and Mayeux, P. (2020) Comprehensive proteomic analysis of murine terminal erythroid differentiation. *Blood Adv*. **4**, 1464-1477.

Gavish, M., Bachman, I., Shoukrun, R., Katz, Y., Veenman, L., Weisinger, G., and Weizman, A. (1999) Enigma of the peripheral benzodiazepine receptor. *Pharmacol. Rev.* **51**, 629–650.

Gnanapragasam, M. N., Mcgrath, K. E., Catherman, S., Xue, L., Palis, J., and Bieker, J. J. (2016) EKLF / KLF1-regulated cell cycle exit is essential for erythroblast enucleation. *Blood* **128**, 1631–1642.

Hanspal, M., and Palek, J. (1987) Synthesis and assembly of membrane skeletal proteins in mammalian red cell precursors. *J. Cell Biol.* **105**, 1417–1424.

Hiroyama, T., Miharada, K., Sudo, K., Danjo, I., Aoki, N., and Nakamura, Y. (2008) Establishment of mouse embryonic stem cell-derived erythroid progenitor cell lines able to produce functional red blood cells. *PLoS ONE* **3**, e1544.

Holm, T. M., Braun, A., Trigatti, B. L., Brugnara, C., Sakamoto, M., Krieger, M., and Andrews, N. C. (2014) Failure of red blood cell maturation in mice with defects in the high-density lipoprotein receptor SR-BI Failure of red blood cell maturation in mice with defects in the high-density lipoprotein receptor SR-BI. *Blood* **99**, 1817–1824.

Ikonen, E. (2008) Cellular cholesterol trafficking and compartmentalization. *Nat. Rev. Mol. Cell Biol.* **9**, 125-138.

Inaba, M., and Maede, Y. (1986) Na, K-ATPase in Dog Red Cells. *J. Biol. Chem.* **261**, 16099–16105.

Inaba, M., and Maede, Y. (1988) A new major transmembrane glycoprotein, gp155, in goat erythrocytes. Isolation and characterization of its association to cytoskeleton through binding with band 3-ankyrin complex. *J. Biol. Chem.* **263**, 17763–17771.

Inaba, M., and Maede, Y. (1989) Inherited persistence of immature type pyruvate kinase and hexokinase isozymes in dog erythrocytes. *Comp. Biochem. Physiol.* **92B**, 151-156.

Ito, D., Koshino, I., Arashiki, N., Adachi, H., Tomihari, M., Tamahara, S., and Inaba, M. (2006) Ubiquitylation-independent ER-associated degradation of an AE1 mutant associated with dominant hereditary spherocytosis in cattle. *J. Cell Sci.* **119**, 3602–3612.

Keerthivasan, G., Small, S., Liu, H., wickrema, A., and Crispino, J. D. (2010) Vesicle trafficking plays a novel role in erythroblast enucleation. *Blood* **116**, 3331-3340.

Kettle, E., Page, S. L., Morgan, G. P., Malladi, C. S., Wong, C. L., Boadle, R. A., and Chircop, M. (2015) A cholesterol-dependent endocytic mechanism generates midbody tubules during cytokinesis. *Traffic* **16**, 1174–1192.

Kiatpakdee, B., Sato, K., Otsuka, Y., Arashiki, N., Chen, Y., Tsumita, T., Otsu, W., Yamamoto, A., Kawata, R., Yamazaki, J., Sugimoto, Y., Takada, K., Mohandas, N., and Inaba, M. (2020) Cholesterol-binding protein TSPO2 coordinates maturation and proliferation of terminally differentiating erythroblasts. *J. Biol. Chem*. in press, doi: 10.1074/jbc.RA119.011679.

Komatsu, T., Sato, K., Otsuka, Y., Arashiki, N., Tanaka, K., Tamahara, S., and Inaba, M. (2010) Parallel reductions in stomatin and Na, K-ATPase through the exosomal pathway during reticulocyte maturation in dogs: stomatin as a genotypic and phenotypic marker of high $K^+$ and low $K^+$ red cells. *J. Vet. Med. Sci.* **72**, 893-901

Konstantinidis, D. G., Pushkaran, S., Johnson, J. F., Cancelas, J. A., Manganaris, S., Harris, C. E., and Kalfa, T. A. (2012) Signaling and cytoskeletal requirements in erythroblast enucleation. *Blood* **119**, 6118–6127.

Lazarides, E., and Moon, R. T. (1984) Assembly and topogenesis of the spectrin-based membrane skeleton in erythroid development. *Cell* **37**, 354–356.

Li, W., Hardwick, M. J., Rosenthal, D., Culty, M., and Papadopoulos, V. (2007) Peripheral-type benzodiazepine receptor overexpression and knockdown in human breast cancer cells indicate its prominent role in tumor cell proliferation. *Biochem. Pharmacol.* **73**, 491–503.

Liu, J., Zhang, J., Ginzburg, Y., Li, H., Xue, F., De Franceschi, L., Chasis, J. A., and An, X. (2013) Quantitative analysis of murine terminal erythroid differentiation in vivo : novel method to study normal and disordered erythropoiesis. *Blood* **121**, 43–50.

Maede, Y., and Inaba, M. (1985) (Na,K)-ATPase and ouabain binding in reticulocytes from dogs with high K and low K erythrocytes and their changes during maturation. *J. Biol. Chem.* **260**, 3337–3343.

Maede, Y., and Inaba, M. (1987) Energy metabolism in canine erythrocytes associated with inherited high $Na^+$- and $K^+$-stimulated adenosine triphosphatase activity. *Am. J. Vet. Res.* **48**, 114–118.

Maede, Y., Inaba, M., and Taniguchi, N. (1983) Increase of Na-K-ATPase activity, glutamate, and aspartate uptake in dog erythrocytes associated with hereditary high accumulation of GSH, glutamate, glutamine, and aspartate. *Blood* **61**, 493–499.

Malik, J., Getman, M., and Steiner, L. A. (2015) Histone methyltransferase Setd8 represses Gata2 expression and regulates erythroid maturation. *Mol. Cell. Biol.* **35**, 2059–2072.

Malik, J., Lillis, J. A., Couch, T., Getman, M., and Steiner, L. A. (2017) The Methyltransferase Setd8 Is Essential for Erythroblast Survival and Maturation. *Cell Rep.* **21**, 2376–2383.

Marginedas-Freixa, I., Alvarez, C. L., Moras, M., Leal Denis, M. F., Hattab, C., Halle, F., Bihel, F., Mouro-Chanteloup, I., Lefevre, S. D., Le Van Kim, C., Schwarzbaum, P. J., and Ostuni, M. A. (2018) Human erythrocytes release ATP by a novel pathway involving VDAC oligomerization independent of pannexin-1. *Sci. Rep.* **8**, 11384.

Marginedas-Freixa, I., Hattab, C., Bouyer, G., Halle, F., Chene, A., Lefevre, S. D., Cambot, M., Cueff, A., Schmitt, M., Gamain, B., Lacapere, J. J., Egee, S., Bihel, F., Le Van Kim, C., and Ostuni, M. A. (2016) TSPO ligands stimulate ZnPPIX transport and ROS accumulation leading to the inhibition of P. falciparum growth in human blood. *Sci. Rep.* **6**, 33516.

Martínez-botas, J., Suárez, Y., Ferruelo, A. J., Gómez-coronado, D., and Lasunción, M. A. (1999) Cholesterol starvation decreases P34 $^{cdc2}$ kinase activity and arrests the cell cycle at G2. *FASEB J.* **13**, 1359–1370.

Maxfield, F. R., and Tabas, I. (2005) Role of cholesterol and lipid organization in disease. *Nature* **438**, 612–621.

Mohandas, N., and Gallagher, P. G. (2008) Red cell membrane: past, present, and future. *Blood* **112**, 3939–3948.

Montagnac, G., Echard, A., and Chavrier, P. (2008) Endocytic traffic in animal cell cytokinesis. *Curr. Opin. Cell Biol.* **20**, 454–461.

Moras, M., Lefevre, S. D., and Ostuni, M. A. (2017) From erythroblasts to mature red blood cells: Organelle clearance in mammals. *Front. Physiol.* **8**, 1–9.

Mukherjee, S., Zha, X., Tabas, I., and Maxfield, F. R. (1998) Cholesterol distribution in living cells: fluorescence imaging using dehydroergosterol as a fluorescent cholesterol analog. *Biophys. J.* **75**, 1915–1925.

Ng, M. M., Chang, F., and Burgess, D. R. (2005) Movement of membrane domains and requirement of membrane signaling molecules for cytokinesis. *Dev. Cell* **9**, 781–790.

Papadopoulos, Vassilios, Baraldi, M., Guilarte, T. R., Knudsen, T. B., Lacapère, J.-J., Lindemann, P., and Gavish, M. (2006) Translocator protein (18kDa): new nomenclature for the peripheral-type benzodiazepine receptor based on its structure and molecular function. *Trends Pharmacol. Sci.* **27**, 402–409.

Papayannopoulou, T., and Migliaccio, A. R. (2017) Chapter 26, Biology of erythropoiesis, erythroid differentiation, and maturation. In *Hematology: basic principles and practice. 7th ed.* (Hoffman, R., Benz, E. J. Jr., Silberstein. L. E., Heslop, H. E., Weitz, J. I., Anastasi, J., Salama, M. E., and Abutalib, S. A., eds.) Elsevier, Philadelphia, PA.

Paulson, R. F., Shi, L., and Wu, D. C. (2011) Stress erythropoiesis: new signals and new stress progenitor cells. *Curr. Opin. Hematol.* **18**, 139–145.

Rone, M. B., Fan, J., and Papadopoulos, V. (2009) Cholesterol transport in steroid biosynthesis: Role of protein-protein interactions and implications in disease states. *Biochim. Biophys. Acta* **1791**, 646–658.

Runz, H., Miura, K., Weiss, M., and Pepperkok, R. (2006) Sterols regulate ER-export dynamics of secretory cargo protein ts-O45-G. *EMBO J.* **25**, 2953–2965.

Rupprecht, R., Papadopoulos, V., Rammes, G., Baghai, T. C., Fan, J., Akula, N., Groyer, G., Adams, D., and Schumacher, M. (2010) *Nat. Rev. Drug Discov.* **9**, 971–988.

Sankaran, V. G., Ludwig, L. S., Sicinska, E., Xu, J., Bauer, D. E., Eng, J. C., Patterson, H. C.,

Metcalf, R. A., Natkunam, Y., Orkin, S. H., Sicinski, P., Lander, E. S., and Lodish, H. F. (2012) Cyclin D3 coordinates the cell cycle during differentiation to regulate erythrocyte size and number. *Genes Develop.* **26**, 2075–2087.

Shalev, H., Kapelushnik, J., Moser, A., Knobler, H., and Tamary, H. (2007) Hypocholesterolemia in chronic anemias with increased erythropoietic activity. *Am. J. Hematol.* **82**, 199–202.

Socolovsky, M. (2007). Molecular insights into stress erythropoiesis. *Curr. Opin. Hematol.* **14**, 215–224.

Swartz, K. L., Wood, S. N., Murthy, T., Ramirez, O., Qin, G., Pillai, M. M., and Minella, A. C. (2016) E2F-2 promotes nuclear condensation and enucleation of terminally differentiated erythroblasts. *Mol. Cell. Biol.* **37**, e00274–16.

Vitols, S., Gahrton, G., Björkholm, M., and Peterson, C. (1985) Hypocholesterolaemia in malignancy due to elevated low-density-lipoprotein-receptor activity in tumour cells: evidence from studies in patients with leukaemia. *Lancet* **2**, 1150–1154.

Yang, H., Wang, H., and Jaenisch, R. (2014). Generating genetically modified mice using CRISPR/Cas-mediated genome engineering. *Nat. Protoc.* **9**, 1956–1968.

Zhang, S., Glukhova, S. A., Caldwell, K. A., and Caldwell, G. A. (2017) NCEH-1 modulates cholesterol metabolism and protects against α-synuclein toxicity in a *C. elegans* model of Parkinson's disease. *Human Mol. Genet.* **26**, 3823–3836.

Zhao, B., Mei, Y., Schipma, M. J., Roth, E. W., Bleher, R., Rappoport, J. Z., and Ji, P. (2016) Nuclear condensation during mouse erythropoiesis requires caspase-3-mediated nuclear opening. *Dev. Cell* **36**, 498–510.

# Acknowledgements

I would like to express my sincere gratitude to my supervisor, Professor Mutsumi Inaba (Laboratory of Molecular Medicine, Graduate School of Veterinary Medicine) for his great guidance throughout this work.

I also express my gratitude to Professor Kazuhiro Kimura (Laboratory of Biochemistry), Professor Mitsuyoshi Takiguchi (Laboratory of Internal Medicine), and Associate Professor Osamu Ichii (Laboratory of Anatomy), all from Graduate School of Veterinary Medicine, for helpful discussion and critical reading of the manuscript, Dr. Narla Mohandas (New York Blood Center) for his enthusiastic support, helpful discussion, and critical reading the manuscript, and Drs. Hongxia Yan, Erjing Gao, and John Hale (all from New York Blood Center) for the effective discussion and technical guidance during my internship at New York Blood Center. Besides, I would like to acknowledge Associate Professor Kensuke Takada (Laboratory of Molecular Medicine), Dr. Kota Sato (National Veterinary Assay Laboratory, Tokyo), Dr. Jumpei Yamazaki (Veterinary Teaching Hospital, Hokkaido University), and all members of the Laboratory of Molecular Medicine for encouragement and technical advises.

Finally, I would like to thank my family, friends, my lovely Labradors (Solo and Money), and Thai community in Hokkaido for the huge support and encouragement during my Ph.D. life.

# Abstract

Erythropoiesis is an essential process that produces sufficient numbers of the enucleated red blood cell (RBC) from the erythroid precursor cell. Previous studies have revealed the mechanisms for various morphologic and biochemical changes during erythropoiesis. However, the factors implicated in regulation of maturation and proliferation in erythroblasts remain yet to be fully defined. Based on an unexpected finding that the HK (high $K^+$) trait characterized with immature RBC phenotypes in dogs is associated with the TSPO2 gene (*TSPO2*) mutations, we previously examined erythropoiesis in HK dogs and found morphological abnormalities in late-stage erythroblasts, suggesting some important roles of TSPO2 in erythropoiesis. TSPO2 (translocator protein 2) is a cholesterol-binding transmembrane protein specifically expressed in late erythroblasts. The purpose of the present study was to investigate the function of TSPO2 in erythropoiesis. To do this, *Tspo2* knockout (*Tspo2*$^{-/-}$) mouse models including *Tspo2*$^{-/-}$ mice and *Tspo2*$^{-/-}$ mouse ES cell-derived erythroid progenitor (MEDEP) cells were generated and the effects of *Tspo2* on erythropoiesis were analyzed. *Tspo2*$^{-/-}$ mice consistently showed impaired cytokinesis with increased binucleated erythroblasts, resulting in compensated anemia and their red cell membranes had increased Na,K-ATPase, resembling the HK phenotype in dogs. *Tspo2*-deficient mouse ES cell-derived erythroid progenitor (MEDEP) cells exhibited similar morphological defects associated with a cell-cycle arrest at the G2/M phase followed by apoptotic cell death, resulting in decreased cell proliferation. *Tspo2*$^{-/-}$ MEDEP cells also exhibited a profound reduction in intracellular unesterified and esterified cholesterol, suggesting the Tspo2 aberration caused cholesterol depletion in erythroblasts. When the terminal maturation was induced, *Tspo2*$^{-/-}$ MEDEP cells showed delays in hemoglobinization, maturation-associated phenotypic changes in CD44, CD71, and TER119 expression, and cell-

cycle progression with no reduction in the number of cell division prior to enucleation. These findings imply that TSPO2 is essential for coordination of maturation and proliferation of late-stage erythroblasts during normal erythropoiesis possibly through regulation of cholesterol availability in erythroblasts. Although TSPO2 has been suggested to have a role in cholesterol redistribution in erythroblasts, the functional sequela of this observation was not defined. The present findings therefore have implicated a major functional role for TSPO2 in erythropoiesis.

# Abstract in Japanese

赤芽球系造血は赤芽球前駆細胞から充分な数の成熟赤血球を生産する生命維持に不可欠の過程である。既に赤芽球造血の間に生じる様々な形態変化や生化学的変化の仕組みが明らかにされている。しかし、赤芽球の成熟と増殖の制御に携わる要因や仕組みには依然として不明が多い。犬には未成熟な表現型の HK（高 $K^+$濃度）型赤血球をもつ個体が存在する。我々のグループは先にこの HK 型形質が TSPO2 遺伝子（*TSPO2*）の変異に起因すること、HK 型犬の骨髄赤芽球造血では後期赤芽球に形態異常が生じることを見出した。この知見は、コレステロール結合膜内在性タンパク質である TSPO2 が赤芽球造血に何らかの重要な役割をもつことを示している。本研究の目的はこの TSPO2 の役割を実証することである。本研究では、*in vivo* のモデルとしてマウス個体の骨髄赤芽球系細胞、*in vitro* のモデルとしてマウス ES 細胞由来赤芽球前駆細胞（MEDEP 細胞）を用い、それぞれの *Tspo2* をノックアウト（*Tspo2*$^{-/-}$）して、その赤芽球造血に対する影響を検討した。*Tspo2*$^{-/-}$マウスの骨髄では細胞質分裂異常による二核、あるいは多核の赤芽球の増加が生じ、軽度の代償性貧血が観察された。末梢血赤血球では Na,K-ATPase 含量の増加が見られ、犬の HK 型赤血球と同様、脱核後も幼弱な赤血球の性質を維持することが示された。*Tspo2*$^{-/-}$MEDEP 細胞は、$G_2$/M 期での細胞周期停止とアポトーシスを伴う細胞質分裂異常と形態異常を呈し、細胞増殖は正常 MEDEP 細胞に比べて著しく低下していた。加えて *Tspo2*$^{-/-}$MEDEP 細胞では細胞内コレステロールが非エステル型、エステル型ともに顕著に減少しており、*Tspo2* の破壊が赤芽球にコレステロール欠乏を生じることが示唆された。エリスロポエチンで赤芽球系分化を誘導した場合、*Tspo2*$^{-/-}$MEDEP 細胞は、ヘモグロビン合成と CD44、CD71、ならびに TER119 の成熟に伴う発現動態に明確な遅滞を示した。また、脱核に至るまでの過程で、細胞分裂回数は正常細胞と同等でありながら細胞周期の進行にも遅れが認められた。これらの知見は、正常な赤芽球造血に TSPO2 の機能が不可欠であり、おそらくはコレステロールの細胞膜への供給を介して後期赤芽球の成熟と増殖を協調的に進行させる役割を担っていることを示唆するものである。